Journal of Cleaner Production 318 (2021) 128642

Contents lists available at ScienceDirect

Journal of Cleaner Production

journal homepage: www.elsevier.com/locate/jclepro

Prediction of emission and performance characteristics of reactivity-controlled compression ignition engine with the intelligent software based on adaptive neural-fuzzy and neural-network

Mehmet Akif Koç [a], Ramazan Şener [b,*]

[a] Department of Mechatronics Engineering, Sakarya University of Applied Sciences, 54187, Sakarya, Turkey
[b] Department of Automotive Engineering, Batman University, 72100, Batman, Turkey

ARTICLE INFO

Handling editor: Panos Seferlis

Keywords:
Reactivity-controlled compression ignition
Adaptive neural-fuzzy inference systems
Artificial neural network
Computational fluid dynamics
Combustion
Methane

ABSTRACT

A fuel reactivity-controlled compression ignition concept promises to overcome increasingly stringent emission standards with ultra-low nitrogen oxide and soot emissions and very high fuel efficiency. In the present work, it was developed an intelligent software-based on adaptive neural-fuzzy inference systems in order to predict the emission and performance values of reactivity-controlled compression ignition engine fueled with natural gas and diesel under different operating conditions through an experimentally validated computational fluid dynamics model with the four cases generated in the study for intelligent software-based on neural-fuzzy systems simulation considering different input and output parameters. The engine model was run at input variables as initial pressure (1.67–2.79 bar), total fuel mass (60–130 mg), exhaust gas recirculation ratio (0–20%), the start of injection (32–56° before top dead center) and total 180 different conditions were generated while output responses such as indicated power, maximum in-cylinder pressure, soot, and nitrogen oxide emissions. The main operating parameters of the reactivity-controlled compression ignition engine were determined for different load conditions, enabling the engine to operate in a wide range with high efficiency and low emission. For the neural-fuzzy inference model presented study, the different number Gaussian curve membership functions (5, 6, 7, 8) (gaussmf) have been used considering different adaptive neural-fuzzy cases, and generally, about 13500 training cycles is found to be optimum neural-fuzzy inference parameters and minimum error value. Mean square error, mean error percentage, and the absolute fraction of variance (R^2) were used to assess and compare the performance of the adaptive neural-fuzzy and artificial neural network. Results of the adaptive neural-fuzzy confirm that the model successfully predicts the performance and emission of the engine with the R^2 value % 99.8, % 99.9, and %96.5 for the output parameters indicated power, maximum in-cylinder pressure, and nitrogen oxide, respectively. Moreover, the performance of the neural-fuzzy inference algorithm compared with artificial neural network and consequently, it was observed that neural-fuzzy inference gives more accurate predict value according to the artificial neural network. Moreover, generating a neural-fuzzy inference architecture using the proposed mathematical foundation given the study shows that neural-fuzzy inference is a very effective and helpful technique to predict the reactivity-controlled compression ignition engine performance and emission parameters.

1. Introduction

Compression ignition (CI) engines are widely used in many application areas such as automotive, railways, power, and marine (Reitz et al., 2020). However, meeting the ever tighter emission limits, different combustion strategies are developed to reduce exhaust emissions and improve efficiency (Mohan et al., 2013). Combustion temperature is one of the substantial factors for NO_X formation (Gao et al., 2021). The major mechanisms of NO_X formation are prompt NO_X and thermal NO_X to be caused by combustion temperature, reaction duration, and oxygen concentration (Huang et al., 2019b). Because higher in-cylinder combustion temperature exceeding 1650 K promotes the oxidation of nitrogen as a thermal NO_X mechanism, it is aimed to reduce NO_X emissions by decreasing combustion temperature (Chen

* Corresponding author.
E-mail address: ramazan.sener@batman.edu.tr (R. Şener).

https://doi.org/10.1016/j.jclepro.2021.128642
Received 8 June 2021; Received in revised form 3 August 2021; Accepted 11 August 2021
Available online 12 August 2021
0959-6526/© 2021 Elsevier Ltd. All rights reserved.

et al., 2020). In addition, it is desired to prevent the formation of soot emission by ensuring a more homogeneous mixture before combustion and by reducing fuel-rich regions (Gehmlich et al., 2018). Thus, an engine with high thermal efficiency and low NO_X and soot emissions will be achieved.

New combustion strategies are being developed to increase efficiency and reduce emissions. One of these new strategies is homogeneous charge compression ignition (HCCI) that premixed air-fuel mixture and high compression ratio ignite the charge and promise very low NO_X and soot emissions (Kimura et al., 2001). Premixed charge compression ignition (PCCI) engines also inject the fuel at the compression stroke (Salahi and Gharehghani, 2019). However, it becomes difficult to control the combustion rate in these strategies, especially at high loads (Mofijur et al., 2019). Moreover, the volume-specific power is limited by excessive combustion rate, and heat release and causes knock, noise, and vibration (Liu et al., 2008). Therefore reactivity-controlled compression ignition (RCCI) engines, which used the auto-ignition characteristics of two different fuels (low and high reactivity) have been proposed (Kokjohn et al., 2011). The ignition delay and combustion duration are controlled by injecting the fuels with two different auto-ignition characteristics into the cylinder as direct and port injection (Nieman et al., 2012). The reactivity stratification is constituted in the cylinder with these two fuels. The low reactivity fuel is premixed with intake air, while the direct injection of the high reactivity fuel is implemented to initiate the low reactivity charge mixture (Pachiannan et al., 2019).

Many different fuels such as gasoline-diesel, gasoline-biodiesel, ethanol-diesel, natural gas-diesel can be used in combination as low and high reactivity fuels in the RCCI engines. Natural gas (predominantly methane) has a lower carbon-hydrogen ratio that emits lower CO_2 emissions with its combustion. Since it does not contain aromatics, soot formation can be suppressed in internal combustion engines (Taqizadeh et al., 2020). Thus, the usage of natural gas in the RCCI engine is promising that producing higher efficiency and power with lower emissions. On the other hand, natural gas is abundant and has relatively low cost besides clean combustion characteristics (Huang et al., 2019a).

Computational fluid dynamics (CFD) modeling is a very useful method for the development of an internal combustion engine (ICE) (Sener et al., 2020). Modeling of an ICE will improve as our comprehension and knowledge of the chemistry and physics mechanism of the phenomena and as computers continue to increase their ability to solve complex equations (Shu et al., 2019). The models describe the thermodynamics, combustion, heat transfer, and emission formation events of the engines (Broatch et al., 2019). Şener and Gül optimized the combustion chamber geometry and injection parameters of the compression ignition engine in order to minimize the exhaust emissions using a multi-objective genetic algorithm (Şener and Gül, 2021). Nazemi and Shahbakhti used Converge CFD code to investigate the injection pressure, spray angle, the start of injection, and the premixed ratio of an RCCI engine on combustion, performance, and emission (Nazemi and Shahbakhti, 2016). Poorghasemi et al. analyzed the performance and emission of the natural gas-fueled RCCI engine for varied injection parameters using Converge CFD code (Poorghasemi et al., 2017). They found that the CFD model can predict the in-cylinder pressure and heat release trends and also exhaust emission with acceptable accuracy.

An artificial neural network (ANN) has been successfully implemented in several problems such as mechanical vibrations (Koide et al., 2014), prediction of the non-linear seismic response of the buildings (Lagaros and Papadrakakis, 2012), modal parameters identification for smart civil structures (Perez-Ramirez et al., 2016), rail rolling (Altınkaya et al., 2014) and estimating some operating parameters in internal combustion engines. ANN is a non-linear and very complicated algorithm performed on computers. Recently, especially with the development of computer technologies, ANN has been successfully applied in defense systems. ANN has been applied to automatic target identification problems in the military field (Rogers et al., 1995). Hosseini and Dalvand estimated the penetration depth of the projectile in a steel block using ANN (M. Hosseini and A. Dalvand, 2014). Some other studies using ANN in the field of defense systems were carried out by (Koç et al., 2016). Furthermore, more detailed literature research has been studied in various engineering fields (Najafi et al., 2018). The adaptive neuro-fuzzy logic inference system (ANFIS), another AI method, is a mixed combination of ANN and fuzzy logic (FL) that uses the learning ability of artificial ANN to obtain fuzzy IF-THEN rules created with appropriate membership functions. ANFIS has been applied in several different engineering fields. For example, the study in which a fire support system was designed using ANFIS was carried out by (Goztepe, 2013). Yadav and Gaur used ANN and ANFIS with the adaptive control for the design of I-IMC to speed control of the uncertain nonlinear heavy-duty vehicle (Yadav and Gaur, 2016). Sada and Ikpeseni studied ANN and ANFIS algorithms to evaluate the performance in terms of predicting machining responses in an AIS steel turning operation (Sada and Ikpeseni, 2021). Intelligent software such as ANN, ANFIS, and Genetic Algorithm have been implemented to an internal combustion engine to evaluate emissions and performance characteristic properties of the engine for different working conditions. The ANN algorithm was performed for the simulate of engine characteristics using ethanol-and kerosene-containing oxygenated fuel (Ebrahimi et al., 2020). The researcher optimizes ANN's performance with GA and particle swarm optimization (PSO) algorithms. Ebrahim et al. have modeled a mathematical computational technique with an ANN algorithm to test the performance of the reactivity controlled ignition (RCCI) engine (Ebrahimi et al., 2018a). Taghavifar et al. investigate the ANN-based prediction of diesel engine exhaust emissions. They trained the ANN model coupled with the CFD approach (Taghavifar et al., 2016). Dharma et al. studied the performance and emission characteristics of diesel direct-injection engines fueled with varying volumetric ratios of Jatropha curcas-Ceiba pentandra biodiesel-diesel blends. They also developed an ANN model in order to predict engine performance and emissions (Dharma et al., 2017). Agbulut et al. examined ANN modeling of the diesel engine fueled with cottonseed methyl-ester in order to predict exhaust emission and engine performance (Ağbulut et al., 2020).

Table 1 summarizes the literature studies about CFD, ANFIS, and ANN approaches. In light of the studies presented above, the highlighted items for the present work have been listed as follows:

- The combustion, performance, and emission values of an RCCI heavy-duty engine fueled with natural gas-diesel were simulated using the experimentally validated CFD model in this study.
- It was generated by simulating a total of 180 cases with different operating parameters.
- The influence of the initial pressure and temperature, methane mass (equivalence ratio), EGR ratio, and the SOI of the direct injection of high reactivity fuel (diesel) as important parameters are investigated on the performance and exhaust emissions of the RCCI engine. Also, indicated power, peak firing pressure, NO_X, and soot emission values were successfully estimated using the ANFIS method.
- Finally, to compare ANFIS performance with another intelligent algorithm, an ANN algorithm architecture has been designed.

From the literature research perspective, one can understand that easily very detailed studies have been performed by scientists on increase engine emission performance using different intelligent software and hybrid models obtained by using their conjunction. The novelty of the presented study is combining computational fluid dynamics finite volume analysis procedure with adaptive neuro-fuzzy and artificial neural network intelligent algorithms to ensure training and testing data which represent emission and performance parameters of the RCCI engine and validate experimental set up according to different cases obtained by considering various emission and engine performance parameter. From the view of the literature studies point, generally, in the studies which use artificial neural approach for predicting of some

Table 1
Overview of the literature review.

Reference	Application Area	Method	Results
Najafi et al. (2016)	SI engine	SVM-ANFIS	The results demonstrate that the SVM and ANFIS are capable of predicting the SI engine performance and emissions. However, the performance of the ANFIS is significantly higher than that of the SVM.
Taghavifar et al. (2016)	CI engine	ANN	CO_2, soot, and NO_X emission of n-heptane fueled CI engine were predicted using ANN. CFD approach was coupled with ANN to train the model.
Dharma et al. (2017)	CI engine	ANN	The performance and emission of the CI engine fueled with Jatropa Curcas-Ceiba Pentandra biodiesel-diesel blends were predicted using the ANN.
Ebrahimi et al. (2018b)	RCCI engine	ANN	Mathematical computational techniques with an ANN algorithm were developed to test the performance of the reactivity-controlled ignition (RCCI) engine.
Ebrahimi et al. (2020)	RCCI engine	ANN-GA-PSO	Based on the RCCI engine's responses derived from the simulation, reactivity-controlled compression-ignition combustion's mathematical model is identified directly using an artificial neural network.
Ağbulut et al. (2020)	CI engine	ANN	The combustion and emission characteristics of the CI engine fueled with different biodiesel blends and injection pressure were successfully predicted using the ANN.
Saravanakumar and Prakash (2020)	CI engine	ANFIS	Effects of the Calophyllum Inophyllum methyl esters fuel blend were investigated using the ANFIS on brake specific fuel consumption, thermal efficiency, and exhaust emissions.
Singh et al. (2020a)	CI engine	ANFIS-GA	Using the ANFIS and genetic algorithm, performance and exhaust emission parameters of the CI engine fueled with biodiesel were precisely forecasted.
Singh et al. (2020b)	CI engine	ANFIS-PSO-GA	In short, the whole study concludes that hybrid techniques like ANFIS-GA and ANFIS-PSO are effective and reliable methods for the effective assessment of engine emission parameters.
Kumar et al. (2021)	CI engine	ANFIS-RSM	The ANFIS model was used to individually correlate the output variable (biodiesel yield) with four input variables with an R2 value of 0.9998.
Atarod et al. (2021)	CI engine	ANFIS-PSO	The applied soft computing combination appears to be a promising approach to model and optimize the operating parameters and fuel composition of diesel engines.

limited emission considering only some restricted cases, the emission, and engine performance parameter has been obtained by laborious and time-consuming experimental study. However, with the using potency of the computational fluid dynamics and adaptive neuro-fuzzy combined algorithm presented in this study, one can easily obtain very critical emission and performance parameters of the RCCI engine without necessary any costly and time-consuming experimental studies. On the other hand, in the recent state-of-art similar studies, the commercial Toolboxes are generally used for adaptive neural-fuzzy applications. This technique is adequate to generate an ANFIS model for basic engineering problems in terms of investigating some basic parameters such as R^2 and mean squared error (MSE) values. But if any researcher wants to some more detail ANFIS parameters such as membership function's midpoint and standard deviation change and consequent parameters given in the study according to iteration number, it is insufficient to use these commercial Toolboxes. The in-house ANFIS special code written in MATLAB has been developed by the authors to investigate more detailed parameters given the presented study such as consequent parameters of each Takaki-Sugeno type IF-THEN rules. Thus, the change of each training and testing pattern given in the study has been presented in detail according to iteration number during the training and testing process.

This research investigated the performance and emission evaluations of natural gas-diesel fueled RCCI engines and explored engine parameters to achieve low NO_X and soot emissions using the experimental, CFD, ANFIS, and ANN techniques. The applications of the RCCI engines would remarkably reduce hazardous pollutants to achieve cleaner production and environmentally friendly on-road and non-road engines.

2. Experimental, CFD, and ANFIS modeling

2.1. CFD modeling

The numerical studies were performed using 3D CFD commercial software Converge (Richards et al., 2019). The computational domains of the RCCI engine with bathtub piston bowl were generated for the CFD simulations (Fig. 1). The piston bowl shape of a heavy-duty diesel engine was optimized for RCCI strategy by (Splitter et al., 2012). RNG k-ε turbulence scheme was adopted to model in the computational domain (Han and Reitz, 1995). Fuel spray was simulated by the Lagrangian-parcel Eulerian-fluid method (Yue and Reitz, 2019). The Kelvin-Helmholtz/Rayleigh-Taylor (KH-RT) breakup model (Beale and Reitz, 1999), no time counter droplet collision (NTC) model (Schmidt and Rutland, 2000), frossling evaporation model (Amsden et al., 1989), O'Rourke turbulent dispersion model (O'Rourke, 1989), and Rebound/Slide spray-wall interaction model (Manuel et al., 1991) were used in the fuel spray process (Table 2).

The SAGE chemistry solver was used with detailed chemical kinetics to model combustion (Senecal et al., 2003). A reduced n-heptane

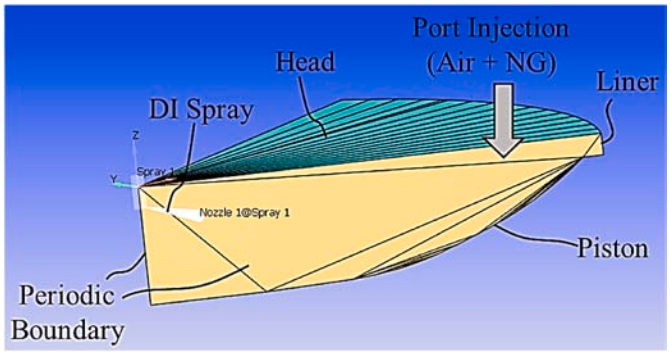

Fig. 1. Computational domain of the RCCI engine with bathtub piston bowl at TDC.

Table 2
Sub-models of the CFD simulation.

Turbulence	RANS - RNG k-ε model
Combustion	SAGE detailed chemistry solver
Reaction mechanism	42 species, 168 reactions
Spray Breakup	KH + RT model
Collision	NTC model
Evaporation	Frossling model
Turbulent dispersion	O'Rourke model
Spray-wall interaction	Rebound/Slide model
Soot	Hiroyasu Soot model
NO_X	Extended Zeldovich model

chemical mechanism includes 76 species and 464 reactions (Nordin, 1998). Diesel and natural gas are represented in the model as C_7H_{16} and CH_4, respectively. The O'Rourke and Amsden model was selected to simulate the wall heat transfer (Amsden, 1997). Hiroyasu Soot model was used to simulate the soot formation. The Extended Zeldovich mechanism was used to simulate NO_X formation (Heywood, 1988).

The CFD simulations were carried out from +125° bTDC to exhaust valve opening (+130° bTDC). The swirl ratio of 0.7 and swirl profile of 3.11 were taken by assuming the initial mixture as homogenous and uniform. A 60-degree sector mesh was used due to the axial symmetrical piston bowl geometry and six equally injector holes. The wall temperatures of the piston, liner, and cylinder head were 575 K, 475 K, and 550 K, respectively.

2.2. Experimental part and validation

The Caterpillar® 3401 single-cylinder DI diesel engine was used as the test engine (Fig. 2). The main specifications of the test engine are listed in Table 3. The common-rail injector with an injection pressure of 50 MPa, a spray angle of 145°, and 6-hole was utilized in the test engine.

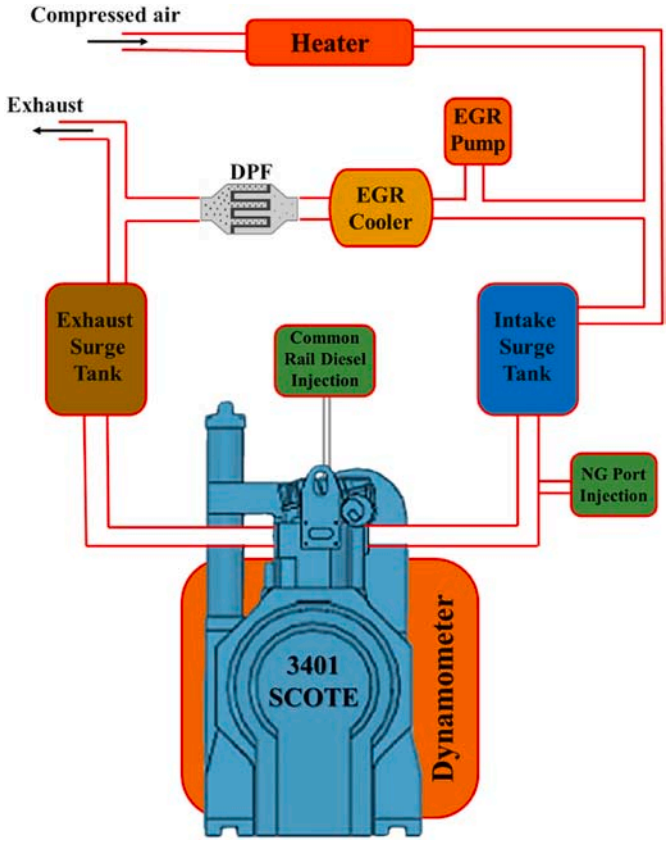

Fig. 2. Test engine laboratory layout.

Table 3
Caterpillar SCOTE 3401E test engine specifications.

Cylinders	Single
Total displacement	2.441 L
Bore x Stroke	137.6 × 165.1 mm
Connecting rod length	261.6 mm
Compression ratio	14.88:1
Direct injection	Diesel
Port injection	Natural gas

The piston bowl geometry was optimized according to the specified spray angle and engine parameters. The start of injection changes from −32° to −56° aTDC and the injector hole diameter is 0.25 mm (Table 4).

The CFD model has been established according to the test engine specifications and operating conditions. In order to validate the CFD model, four cases were defined with different indicated gross indicated mean effective pressure ($IMEP_g$) and intake pressure (Table 5). The engine speed was set to 1300 r/min. and the direct injection of diesel fuel to 13 mg/cycle. The model was calibrated by comparing the results obtained by experimental (Walker et al., 2015) and simulation (Ebrahimi et al., 2018b) with in-cylinder pressure and rate of heat release values. Prediction of the starting point and the ending point of combustion of the CFD model was an acceptable level, differences were not more than 2° crank angle for cases 1–4 (Fig. 3). The CFD model predicted faster heat release during premixed combustion phases. This may be due to the representation of natural gas and diesel, simplified reaction mechanism, and inaccuracy of modeling of the spray. Furthermore, there is an error in the measurement of the tests (Chen et al., 2020). According to the studies, the CFD results can be used as supplying data for ANFIS and ANN approach to predict the characteristics of the RCCI engine.

The in-cylinder equivalence contours of the validation cases on the cut plane of the spray axis are illustrated in Fig. 4. The increase of the methane mass for cases causes the enhancement of the equivalence ratio. Because of the increment of methane mass in the premixed charge, and enhancement of the homogeneity of the equivalence ratio inside the cylinder, local fuel rich zones decrease. The same statement conduces the increment in in-cylinder temperature distribution (Fig. 5).

2.3. Mesh independency

Since the test engine has a 6-hole injector, a 60-degree sector mesh was utilized to minimize CPU cost. The mesh size is very important for both solution accuracy and simulation time in CFD simulation studies. The mesh size should be chosen so that the results can be obtained in the most accurate way in a reasonable time. The mesh independence studies were performed to ensure that the findings were independent of the mesh size.

The model was performed using three different mesh sizes as fine (1.5-mm), medium (1.8-mm), and coarse (2.3-mm). The adaptive mesh refinement (AMR) method was adopted at embedding levels of two according to velocity and temperature fluctuations during the simulation. Also, fixed embedding levels of two were applied to the spray region. Fixed embedding and AMR layers of the three mesh sizes were the same except for the base grid size.

Table 4
Operating parameters of the engine model.

IVC	−143° aTDC
EVO	+135° aTDC
Swirl ratio	0.7
Injector hole diameter	0.25 mm
Number of injector holes	6
Injector spray angle	145 deg.
SOI timing	32°–56° bTDC

Table 5
Operating parameters of the validated cases.

	Case-1	Case-2	Case-3	Case-4
IMEP$_g$ [bar]	7.7	9.4	11.5	13.5
Speed [r/min]	1300	1300	1300	1300
Intake Pressure [bar]	1.32	1.60	1.90	2.20
SOI (diesel) [° bTDC]	42	45	48	51
Diesel mass [mg]	13	13	13	13
Methane mass [mg]	62	76	96	108
EGR [%]	0	0	0	0

The pressure and rate of heat release curves of all three meshes had similar trends (Fig. 6). The fine mesh estimated the ignition delay value more accurately, but it increased the CPU cost. The results of the coarse mesh had inconsistency around the premixed combustion region. Emission values of medium and fine mesh size were very close (Fig. 6c). Therefore, medium mesh with a 1.8-mm grid size was accepted with an AMR level of 2. Thus, the total cell number can increase up to $1.1 \times 10^{+4}$ during the simulation.

2.4. ANFIS modeling

Jang (1993) proposed the ANFIS system that combines learning ability with decision-making ability. The structure of the ANFIS model is considered a combination of fuzzy inference systems (FIS) and ANN. Apart from that, it uses the "Takagi-Sugeno" inference model, which uses IF-THEN rules to correlate inputs and outputs. This feature enables ANFIS to cope better with the real data incoming from the outside world due to its high learning ability. ANFIS is very efficient in terms of calculation technique and is widely used in modeling nonlinear systems. It is an important disadvantage that ANN and FL are dependent on expert knowledge on issues such as creating the topology of the network, selecting membership function (MF), and determining MF parameters. The approach of combining FL with ANN makes the problem less dependent on expert knowledge. Due to this feature, ANFIS has been successfully applied in several different engineering fields such as predicting biochar yield (Ewees et al., 2017), estimating wind speed (Ahmed et al., 2017), estimating copper prices (Alameer et al., 2019), and forecasting fuel consumption (Al-qaness et al., 2019).

2.4.1. ANFIS forward-propagation learning algorithm

Fig. 7 shows the ANFIS architecture used to predict emissions and performance parameters of the RCCI engine used in this study for different input parameters initial pressure (IP), total fuel mass (TFM), exhaust gas recirculation (EGR), and the start of injection (SOI) for diesel fuel. As seen in Fig. 7, indicated power (IKW), peak firing pressure (PFP), Soot, and nitrogen oxide (NO_X) were determined as the output parameters for ANFIS considering different simulation cases. According to Fig. 7, ANFIS architecture consists of six layers. Each layer consists of several neurons determined by neuron functions. Let us assume that in a four-input (*x, y, z, t*) parameters system, fuzzification of the parameters *x, y, z, t* are represented by N_A, N_B, N_C, N_D MFs respectively. In this case, N_R is the number of rules, $N_R = N_A \times N_B \times N_C \times N_D$ number of rules are written in Takaki-Sugeno type IF-THEN form to define the relation between ANFIS input parameters and output parameters as shown in Equation (1):

$$\begin{cases} \{R^1 : if\ \ x\ \ is\ \ A_1,\ \ y\ \ is\ \ B_1,\ \ z = C_1\ \ and\ \ t = D_1,\ \ then\ \ f^1 = p_1x + q_1y + r_1z + k_1t + u_1 \\ \{R^2 : if\ \ x\ \ is\ \ A_2,\ \ y\ \ is\ \ B_2,\ \ z = C_2\ \ and\ \ t = D_2,\ \ then\ \ f^2 = p_2x + q_2y + r_2z + k_2t + u_2 \\ \vdots \\ \{R^{N_R} : if\ \ x\ \ is\ \ A_{N_A},\ \ y\ \ is\ \ B_{N_B},\ \ z = C_{N_C}\ \ and\ \ t = D_{N_D},\ \ then\ \ f^{N_R} = p_{N_R}x + q_{N_R}y + r_{N_R}z + k_{N_R}t + u_{N_R} \end{cases} \quad (1)$$

In Equation (1) p_i, q_i, r_i, k_i and u_i are the consequent parameters, which are determined during the training of ANFIS.

The layers within ANFIS are as follows:

- ***Layer 1***: Each neuron in this layer is input neurons where input signals are transferred to other layers.
- Layer 2: In an ANFIS model with two inputs given in Fig. 7, the output of the second layer is calculated as follows (the first input to be graded with *n* MF functions and the second input to be graded with *m* possessive functions).

$$O_i^2 = \mu_{\Phi i}(x), \left\{ \begin{matrix} i = 1, .., N_{A,B,C,D} \\ \Phi = \{A, B, C, D\} \end{matrix} \right\} \quad (2)$$

If the Gaussian membership function with a maximum of 1 and a minimum of 0 is used as membership function on each neuron, the result function is written as follows:

$$\mu_{\Phi i}(x) = \exp\left[- \left(\frac{\Psi - m_i}{\sigma_i} \right)^2 \right], \quad \left\{ \begin{matrix} i = 1, .., N_{A,B,C,D} \\ \Psi = (x, y, z, t) \end{matrix} \right\} \quad (3)$$

In Equation (3) parameters m_i and σ_i represent the midpoint and standard deviation of the Gaussian membership function, respectively. These variables are adjusted while training ANFIS.

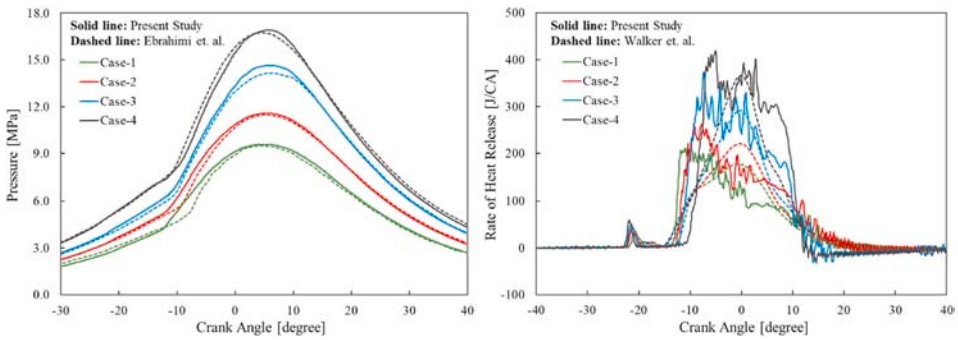

Fig. 3. Comparison of experiment and simulation cylinder-averaged pressure traces.

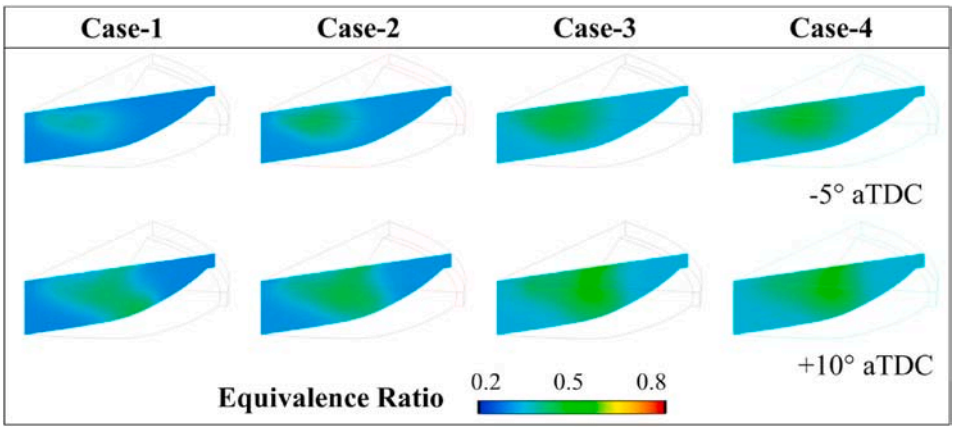

Fig. 4. In-cylinder equivalence ratio distribution for four cases at −5° and +10° aTDC.

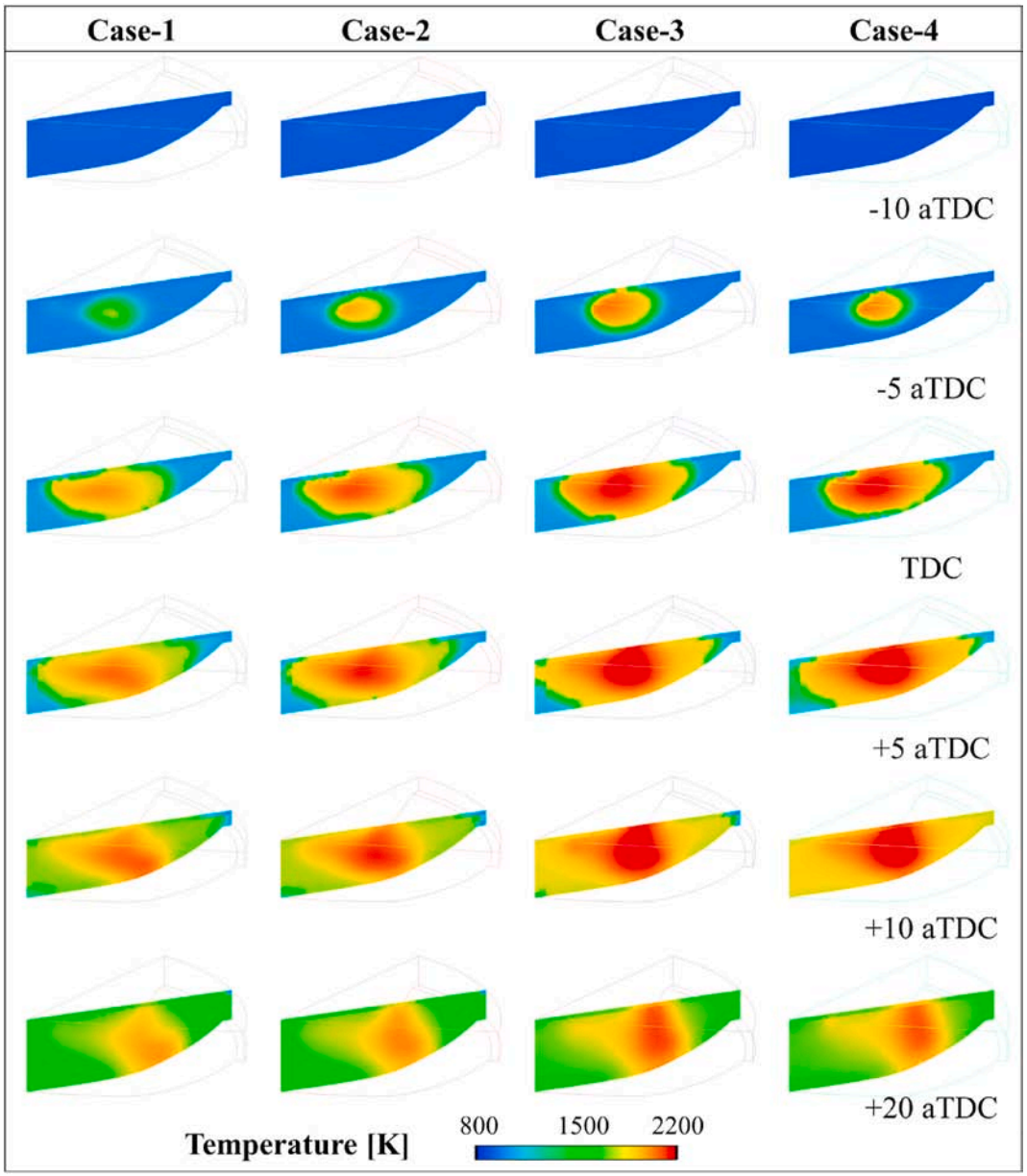

Fig. 5. In-cylinder temperature distribution for four cases at different crank angles.

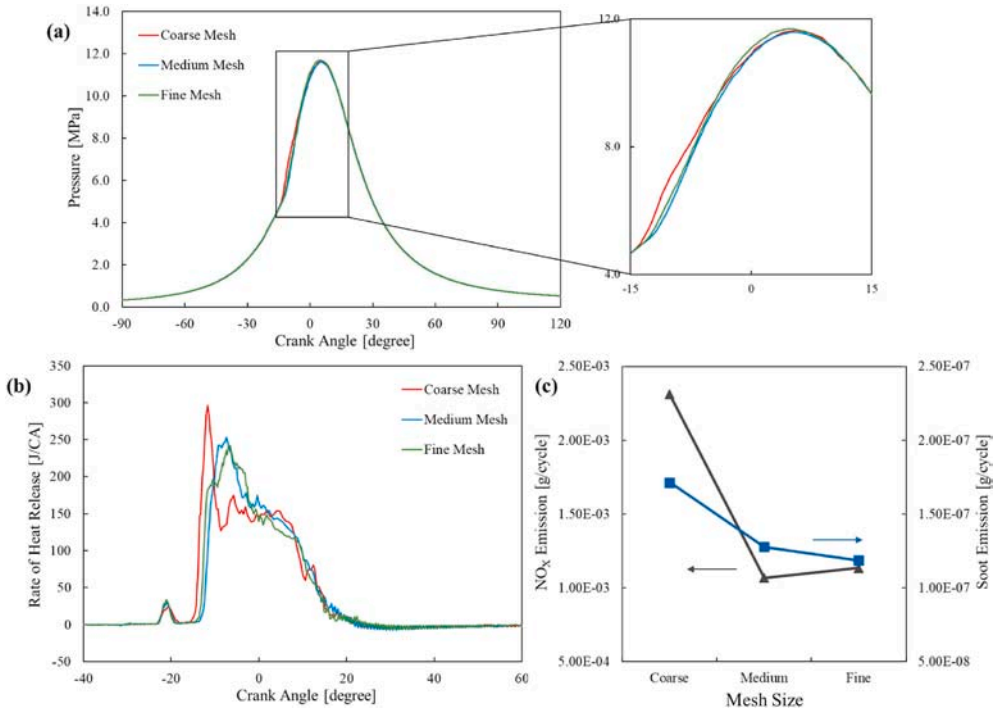

Fig. 6. Comparison of in-cylinder a) pressure traces, b) rate of heat release, c) emissions of three different mesh sizes.

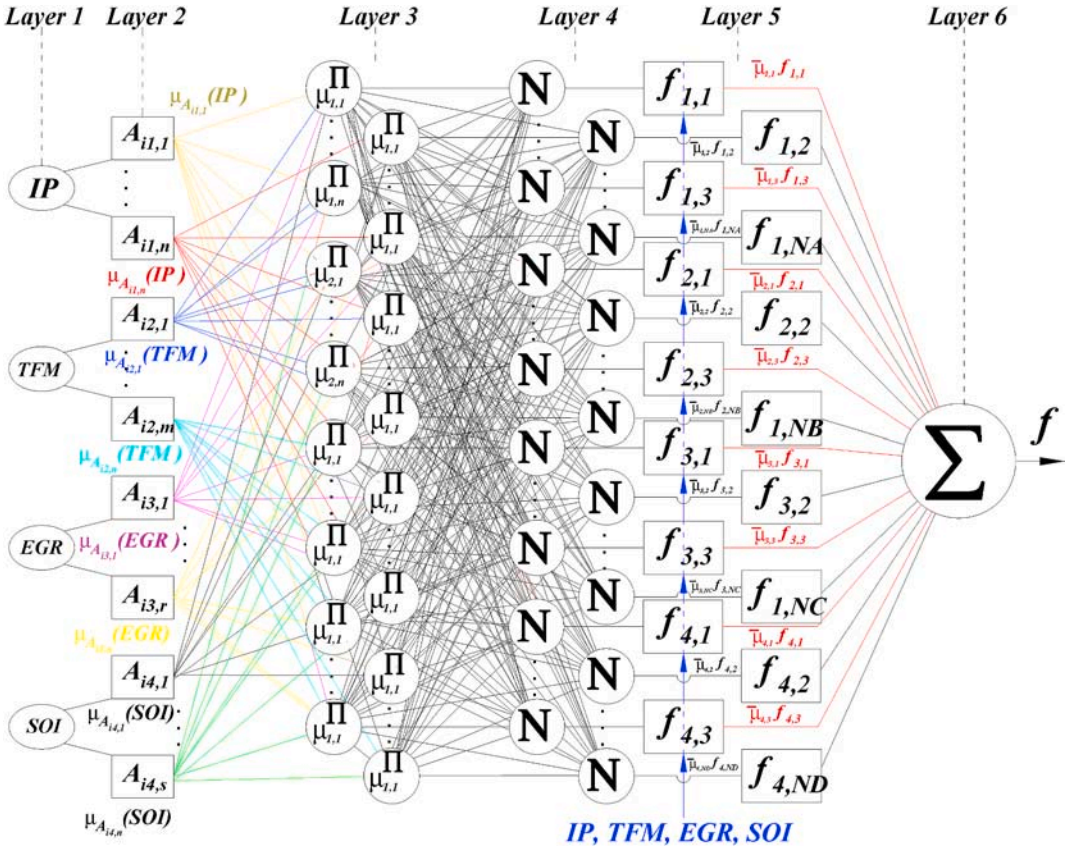

Fig. 7. ANFIS architecture used in this study with four inputs parameters *IP, TFM, EGR,* and *SOI,* and one output parameter.

- ***Layer 3***: Each neuron at this layer is tagged with ∏ and shows the multiplication of all entering signs.

$$O_i^3 = \mu_i = \mu_{A,i}(x)\mu_{B,j}(y)\mu_{C,k}(y)\mu_{D,r}(y), \left\{ \begin{array}{ll} i = 1,..,N_A & k = 1,...,N_C \\ j = 1,...,N_B & r = 1,...,N_D \end{array} \right\} \quad (4)$$

- ***Layer 4***: In this layer, each neuron is enabled with **N**, and the normalized firing level of each rule is calculated as follows:

$$O_i^4 = \overline{\mu}_i = \frac{\mu_i}{\sum_{j=1}^{N_R} O_j^3}, \quad i = 1, \ldots, N_R \tag{5}$$

- ***Layer 5***: Every neuron i in this layer is an adaptive neuron with the neuron function. The neuron exit function is calculated as follows:

$$O_i^5 = \overline{\mu}_i f_i = \overline{\mu}_i (p_i x + q_i y + r_i z + k_i t + u_i), \quad i = 1, \ldots, N_R \tag{6}$$

- ***Layer 6***: There is only one neuron in this layer, and it is enabled with **∑**. Here, the outputs obtained from the fifth layer are summed and ANFIS output is obtained as follows:

$$O^6 = f = \sum_i \overline{\mu}_i f_i = \frac{\sum_i \mu_i f_i}{\sum_i \mu_i} \tag{7}$$

2.4.2. ANFIS back-propagation learning algorithm

In the backpropagation learning algorithm, the error value obtained from the output of the network is reflected the input layer and the necessary weight variables are adjusted. The error obtained from the output of the network is calculated as follows:

$$e = d - f \tag{8}$$

In Equation (8), the parameter d is the expected output value corresponding to any x, y input set given to ANFIS. Other than that, f is the actual output value of the network. By applying the least-squares method to this error value, the error criterion E is calculated as follows:

$$E = \frac{1}{2} e^2 \tag{9}$$

The error value for the output of the ANFIS model, also *MSE*, the absolute fraction of variance $R^2$and mean error percentage (*MEP*) are respectively expressed as follows:

$$MSE = \frac{1}{N_p} \sum_{i=1}^{N_p} (f_i - d_i)^2, \quad R^2 = 1 - \left(\frac{\sum_{i=1}^{N_p} (f_i - d_i)^2}{\sum_{i=1}^{N_p} f_i^2} \right), \quad MEP = \frac{\sum_{i=1}^{N_p} \left(\frac{d_i - f_i}{d_i} \right) x100}{N_p}, \tag{10}$$

The parameter N_p in Equation (10) represents the number of samples in the training or test set. Using the error criterion, the error is reflected layer by layer as shown in Appendix A.

3. Simulation cases and results

In this study, the four different simulation cases given in Table 6 have been introduced to test the performance of the ANFIS model which is designed for RCCI engine emissions and performance parameters and given in Fig. 7. In all of the cases, the parameters IP, TFM, EGR, and SOI have been represented as input parameters of the ANFIS model. On the other hand, the parameters IKW, PFP, Soot, and NO_X have been assigned as output parameters for cases 1 to 4, respectively. For the fuzzification of the input parameter given in Table 6, four various MF numbers have been considered as shown in Table 7 to evaluate the effect of the MF number upon ANFIS predict performance. Accordingly, the performance of each case given in Table 6 has been evaluated considering four MF numbers given in Table 7. The number of the rules determined according to the number of the MF which used fuzzification the input parameters has been given in the sixth row of Table 7. Moreover, in the last row in Table 7, the type of MF used in this study has been given.

Table 6
Simulation cases used in this study.

	Inputs				Output
Case 1	IP	TFM	EGR	SOI	IKW
Case 2	IP	TFM	EGR	SOI	PFP
Case 3	IP	TFM	EGR	SOI	Soot
Case 4	IP	TFM	EGR	SOI	NO_X

Table 7
Simulation cases used in this study.

	MFs 5	MFs 6	MFs 7	MFs 8
MF number for input 1	5	6	7	8
MF number for input 2	5	6	7	8
MF number for input 3	5	6	7	8
MF number for input 4	5	6	7	8
Number of Rules (RN)	625	1296	2401	4096
Type of MF	Gaussian	Gaussian	Gaussian	Gaussian

Table 8
The training data sets used in this study for the projectile mass and projectile exit velocity obtained by FEM.

	IP	TFM	EGR	SOI	IKW	PFP	SOOT	NO_X
1	1.67	72.8	0	32	16.53	86.48	0.00097	0.927
2	2.41	111.0	0	32	30.56	136.9	0.00026	0.738
3	1.67	69.8	5	32	18.41	86.35	0.00078	0.618
4	2.41	106.1	5	32	29.31	123.9	1.79e-5	0.685
5	1.67	69.2	10	32	16.86	84.44	0.00037	0.619
6	2.41	101.2	10	32	27.79	119.3	4.34e-5	0.545
7	1.67	63.83	15	32	13.29	79.85	0.00145	0.619
8	2.41	96.32	15	32	25.89	115.4	0.00068	0.369
9	1.67	60.84	20	32	11.86	77.95	0.0012	0.511
10	2.41	91.42	20	32	15.97	109.1	0.00093	0.506
11	1.67	72.80	0	35	18.36	90.40	0.00032	0.749
12	2.41	111.0	0	35	30.44	134.9	5.57e-6	0.791
13	1.67	69.81	5	35	19.10	88.13	0.00042	0.511
14	2.41	106.1	5	35	29.33	130.3	1.1362	0.72
15	1.67	69.27	10	35	18.75	87.27	0.00069	0.477
16	2.41	101.2	10	35	27.79	117.9	2.5e-5	0.557
17	1.67	63.83	15	35	16.43	82.87	0.00077	0.356
18	2.41	96.32	15	35	26.37	116.0	8.6e-5	0.384
19	1.67	60.84	20	35	12.77	78.69	0.00092	0.380
20	2.41	91.42	20	35	21.73	115.1	0.00064	0.217
21	1.67	72.80	0	41	19.64	93.51	5.27e-5	0.455
22	2.41	111.0	0	41	30.85	145.1	0.00010	0.401
23	1.67	69.81	5	41	19.45	96.29	0.00069	0.196
24	2.41	106.1	5	41	29.70	147.6	1.54e-5	0.422
25	1.67	69.27	10	41	19.18	90.34	0.00023	0.285
26	2.41	101.2	10	41	28.57	140.4	3.47e-5	0.175
27	1.67	63.83	15	41	17.23	84	0.00037	0.179
28	2.41	96.32	15	41	27.07	133.1	0.00012	0.140
29	1.67	60.84	20	41	16.20	81.79	0.00069	0.085
30	2.41	91.42	20	41	24.26	115.8	0.00049	0.069

3.1. Training of ANFIS

Training an ANFIS model means reducing the difference between the ANFIS output obtained against each sample given as input to ANFIS during the training and the actual output below the predetermined error tolerance. For this purpose, sixty pieces of pattern used in this study to train the ANFIS model have been given some training pattern in Table 8. In these patterns, two different values {1.67, 2.41} for IP parameter, ten different value intervals [72, 111] for TFM value, five different values {0, 5,10,15,20} for EGR parameter, six different values {32,35,41,44,50,56} for SOI parameter have been selected for the ANFIS simulation considering four cases given in Table 6. The training process is completed by changing the consequent parameters given by Equation (1) and determined for each rule (p_i, q_i, r_i, k_i, u_i) and MF midpoint and gradient parameters in MF statements given in Equations (5a-b) at each

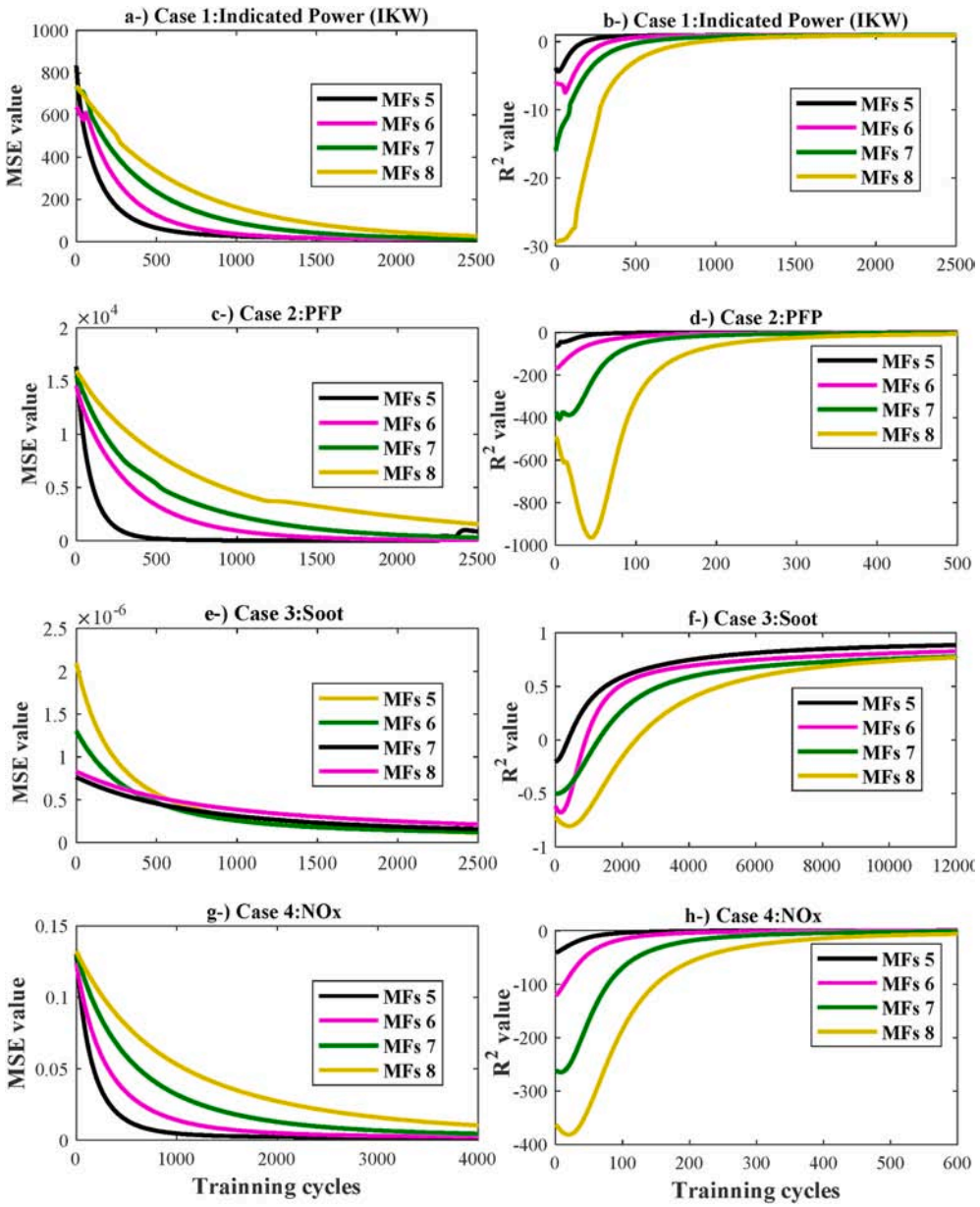

Fig. 8. The error value for the different cases a-) MSE value for Case 1, b-) R^2 value for Case 1, c-) MSE value for Case 2, d-) R^2 value for Case 2, e−) MSE value for Case 3, f-) R^2 value for Case 3, g-) MSE value for Case 4, h-) R^2 value for Case 4.

training iteration and adjusting them to minimize error.

The training process consists of 13500 training cycles. As there are 120 cases in each training set, each training cycle consists of 120 iterations. Fig. 8a-h shows the change of *MSE* and R^2 values for four different cases given in Table 6 and four different MFs respectively depending on the number of iterations. As seen in Fig. 8, as the number of training cycles increases, the *MSE* value gradually decreases. However, as the number of training cycles increases, it is seen that the R^2 value gradually approaches 1. Apart from this, as seen in Fig. 8, as the number of MF used for the fuzzification of the input values in the second layer and the number of rules determined accordingly, the gradient of the *MSE* and R^2 graphic generally decreases. For example, as seen in Fig. 8a, the *MSE* value was obtained as 210.4 at the end of 200 iterations for MFs 5 in Case 1, while this value was determined as 550.4 for MFs 8 in Case 1. On the other hand, R^2 value was obtained as 0.1331 at the end of 200 iterations for MFs 5 in Case 1, while this value was obtained as −17.39 for MFs 8 in Case 1.

In Table 9, the error and *MSE* values obtained in different training cycles are given for some patterns in the training set, considering the four cases given in Table 6 and four different MFs given in Table 7. As seen in Table 9, for all training sets, the error value decreases as the number of training cycles increases. In addition, as the number of training cycles increases, the *MSE* values of the samples in the training set decrease significantly, while the R^2 value gradually increases and approaches 1. As can be seen in Table 9, there is no linear relationship between the number of MF used for the fuzzification of the input parameters and the number of rules obtained based on them, and the *MSE* and R^2 values. Especially at low iteration numbers, the increase in the MF number caused an increase in the MSE value, while the R^2 value gradually decreased. However, when the high iteration number is reached, the situation is reversed. In addition, Fig. 9 shows the variation in error value for all examples in the training set depending on the number of training cycles.

In Fig. 10, the comparison of the values produced by ANFIS at the end of 13500 training cycles against the examples in the training set for four different cases given in Table 6 and the actual values obtained from

Table 9
The error of the training pattern for the different cases and different training rounds.

Itr nmbr			*MSE*	R^2	Training Pattern number							
					15	30	45	60	75	90	105	120
500	Case 1	MFs 5	65.47	0.867	1.48	8.69	7.88	5.01	0.07	3.71	0.33	15.73
	Case 2	MFs 5	189.1	0.985	6.92	26.9	24.6	14.8	0.5	14.0	15.0	11.2
	Case 3	MFs 5	5.69e-7	0.089	6.5e-5	0.00016	0.0002	0.00031	0.00039	0.00044	0.001	0.0014
	Case 4	MFs 5	0.01399	0.8163	0.0803	0.0577	0.0751	0.0728	0.0849	0.0265	0.0652	0.01199
	Case 1	MFs 6	126.4	0.58	8.33	15.93	1.36	10.8	14.7	13.7	6.53	3.086
	Case 2	MFs 6	3325.3	0.256	49.6	56.26	56.3	60.7	69.0	59.3	65.4	67.39
	Case 3	MFs 6	4.6e-7	−0.44	0.0003	0.00032	0.0014	0.0004	0.0002	0.0004	4.81e-5	0.00037
	Case 4	MFs 6	0.033	0.213	0.2	0.183	0.046	0.052	0.0809	0.0082	0.0076	0.0302
	Case 1	MFs 7	236.6	−0.259	19.6	22.8	18.8	22.0	17.9	15.2	18.2	10.18
	Case 2	MFs 7	5326.5	−0.964	73.63	74.39	69.2	80.7	80.7	88.1	63.1	73.17
	Case 3	MFs 7	4.57e-07	−0.39	0.00087	0.0001	0.0007	0.00012	0.00069	0.00018	0.00010	4.331e-5
	Case 4	MFs 7	0.058	−2.049	0.26	0.25	0.091	0.0472	0.01066	0.014	0.019	0.084
	Case 1	MFs 8	334.1	−2.83	19.5	13.0	11.1	24.6	22.6	20.4	14.0	14.78
	Case 2	MFs 8	8184.87	−6.65	92.2	82.7	73.5	102	106	89.9	75.8	87.18
	Case 3	MFs 8	5.29e-07	−0.79	0.00022	0.00041	0.0006	0.00010	0.00082	0.00060	0.00046	0.00063
	Case 4	MFs 8	0.08025	−8.436	0.314	0.306	0.132	0.00974	0.01097	0.0133	0.00249	0.025
7000	Case 1	MFs 5	2.93	0.99	2.42	1.5	0.34	1.95	1.76	2.02	0.73	1.13
	Case 2	MFs 5	9.19	0.99	1.86	2.39	2.74	2.7	2.46	0.40	1.84	1.54
	Case 3	MFs 5	5.03e-8	0.83	0.00026	7.23e-5	0.0002	9.02e-5	2.81e-6	0.00025	0.00026	2.77e-5
	Case 4	MFs 5	0.0013	0.98	0.04	0.084	0.064	0.026	0.026	0.021	0.013	0.0076
	Case 1	MFs 6	4.564	0.993	0.31	1.29	5.1	2.88	1.13	2.14	3.23	0.647
	Case 2	MFs 6	9.348	0.999	1.02	2.266	2.86	2.46	3.10	0.91	4.84	2.280
	Case 3	MFs 6	7.08e-08	0.76	0.00020	7.65e-5	0.0004	6.5e-5	2.06e-5	5.8e-5	0.00063	0.00024
	Case 4	MFs 6	0.0017	0.98	0.04	0.083	0.0908	0.029	0.037	0.02	0.0081	0.0012
	Case 1	MFs 7	3.22	0.99	1.81	2.29	2.86	0.29	1.32	1.96	0.56	0.0105
	Case 2	MFs 7	15.07	0.99	0.77	4.286	7.22	2.13	3.25	5.24	3.90	1.53
	Case 3	MFs 7	8.36e-8	0.709	0.00028	0.00028	0.0003	8.1e-7	0.00016	0.00038	0.0007	0.00022
	Case 4	MFs 7	0.0025	0.979	0.031	0.064	0.12	0.055	0.033	0.014	0.0094	0.013
	Case 1	MFs 8	3.93	0.993	0.64	0.997	1.02	1.59	0.31	1.45	1.36	2.64
	Case 2	MFs 8	67.72	0.995	3.11	11.71	13.2	6.04	9.64	12.3	13.3	1.61
	Case 3	MFs 8	9.29e-8	0.64	0.00024	4.6e-5	0.0003	5.52e-6	0.00050	0.00018	0.00043	0.00038
	Case 4	MFs 8	0.004	0.95	0.0233	0.013	0.12	0.052	0.067	0.019	0.0085	0.0032
13500	Case 1	MFs 5	1.23	0.998	2	1.58	0.036	1.22	0.47	1.753	0.252	0.692
	Case 2	MFs 5	6.93	0.999	1.891	1.345	0.886	2.482	1.274	0.456	0.947	1.2756
	Case 3	MFs 5	3.2e-8	0.894	0.00020	1.16e-6	0.0003	0.00017	4.1e-5	0.00031	0.00025	8.843e-6
	Case 4	MFs 5	0.001	0.990	0.03	0.081	0.0566	0.025	0.027	0.012	0.00363	0.0052
	Case 1	MFs 6	2.79	0.995	0.63	0.079	0.11	1.19	0.81	0.17	1.48	0.541
	Case 2	MFs 6	6.901	0.999	0.508	1.972	2.08	2.57	3.51	0.525	3.29	0.895
	Case 3	MFs 6	4.85e-8	0.838	7.34e-5	0.00010	0.0003	2.69e-5	8.9e-6	0.00012	0.00053	0.000209
	Case 4	MFs 6	0.0014	0.988	0.045	0.0894	0.071	0.028	0.0278	0.0179	0.0089	0.00637
	Case 1	MFs 7	1.72	0.997	1.89	2.27	1.855	0.733	1.811	1.52	0.465	0.872
	Case 2	MFs 7	8.62	0.999	1.14	2.908	3.16	2.08	0.971	1.85	0.023	1.66
	Case 3	MFs 7	5.99e-8	0.7912	0.00022	0.00027	0.0003	9.64e-5	0.00010	0.00048	0.00063	0.00012
	Case 4	MFs 7	0.0017	0.985	0.05058	0.083	0.0929	0.042	0.02038	0.02346	0.016	0.0039
	Case 1	MFs 8	1.93	0.997	0.833	0.204	1.54	0.614	0.104	0.753	0.956	1.98
	Case 2	MFs 8	12.21	0.999	1.03	3.69	4.65	1.33	2.31	2.83	3.88	2.93
	Case 3	MFs 8	5.92e-8	0.787	0.00027	2.27e-5	0.0003	0.00010	0.00029	0.00037	0.00056	0.000204
	Case 4	MFs 8	0.0023	0.981	0.0253	0.0641	0.118	0.038	0.0489	0.00091	0.00482	0.005

the CFD model introduced in section 2 are given. As seen in Fig. 10, the ANFIS output closest to the actual output of the samples in the training set using CFD was obtained in MFs 5 given in Fig. 10a. This situation arises from the fact that the lowest *MSE* (1.23) value and the highest R^2 (0.998) value obtained as a result of 13500 training cycles, as given in Table 9, is obtained in MFs 5. Apart from this, it is seen that the output produced by the ANFIS model in MFs 6 is quite different from the actual output of CFD. This situation shows that while trying to solve an engineering problem with the ANFIS model, the topology of the network should be adjusted well by the designer. So, using too much MF or too little MF may not always work best for solving every problem. In this case, the designer should determine the most appropriate ANFIS topology by examining the effect of different membership functions on ANFIS performance. Fig. 11 shows the comparison between ANFIS output which has been obtained considering four different MFs given in Table 7 for Case 2 given in Table 6 and CFD training value. As shown in Fig. 11, the closest value of the ANFIS model's produced output to CFD value has been obtained in MFs 5 given in Table 7. Besides, Figs. 12 and 13 show a comparison of the ANFIS output value at end of the training process with CFD value for Case 3 and 4 considering training sets, respectively. In Tables 10 and 11, the consequent coefficients of the rule output functions obtained by using four different MFs as a result of 13500 training cycles are given.

3.2. Testing of ANFIS

In order to evaluate the performance of the ANFIS model which was completed the training with the examples in the training set listed in Table 9, it was tested using different patterns that are not included in the training set. Thus, a total of 60 patterns was used to evaluate the performance of the ANFIS model and only shown 30 patterns in Table 12. The selected test parameters must be in the same search space as the training sets considering a high ANFIS performance. If the selected test parameters and the training set are in different search spaces, there is a risk for a low ANFIS performance.

In Table 13, the relative error of each sample is shown for the total of 60 parameters in the testing set, taking into account the five different cases given in Table 6. The relative error for each sample in the test set is

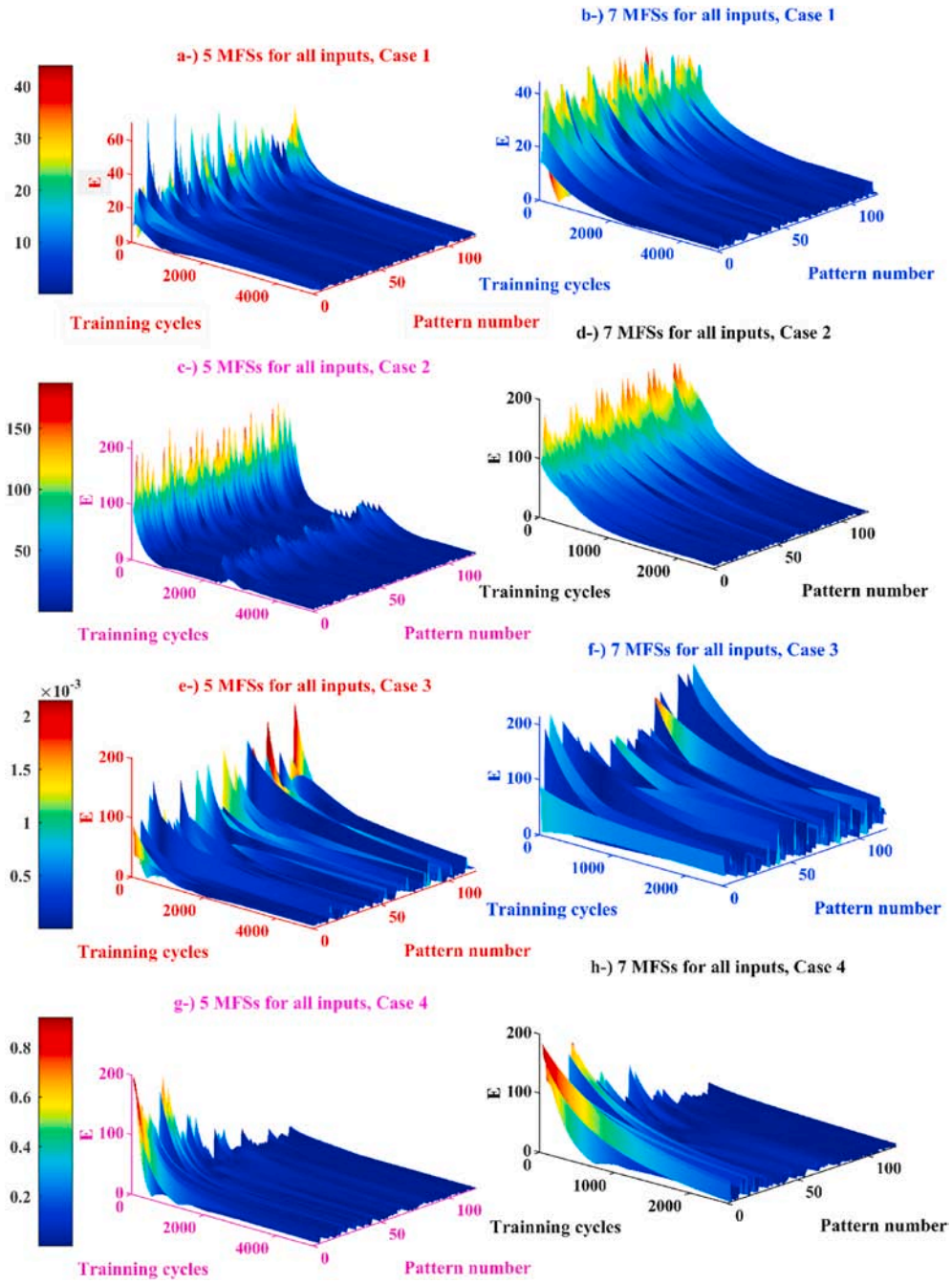

Fig. 9. The error value change of the pattern in the training set according to training cycle a-) 5 MFs Case 1, b-) 7 MFs Case 1, c-) 5 MFs Case 2, d-) 7 MFs Case 2, e−) 5 MFs Case 3, f-) 7 MFs Case 3, g-) 5 MFs Case 4, h-) 7 MFs Case 4.

calculated as follows:

$$\varepsilon_i = \frac{|E|}{B}100 \tag{32}$$

As seen in Table 13, Case 3 has the lowest ANFIS test performance due to the highest relative error considering the ANFIS testing results using the test set given in Table 12. Because the training performance of Case 3 given in Fig. 12 is low and the lowest R^2 value given in Table 9 is obtained in Case 3. On the other hand, the R^2 value for Case 3 was obtained as 0.89, 0.83, 0.79, and 0.78 after 13500 training cycles for the MFs 5–8 analyzes, respectively (Table 9). Otherwise, the minimum relative error for all samples in the testing set was obtained in Case 2 (Table 13). It can clearly be seen in Table 9 the reason for these results. The highest R^2 value for all samples included in the testing set was 0.999, 0.999, 0.999, 0.999 for the MFs 5–7 analyzes in Case 2, respectively. It is seen in Fig. 11 that the closest output to all samples in the training set for four different MFs 5–8 analyzes is given in Case 2. In Figs. 14-17a-d, the comparison of the ANFIS results and the samples in the testing set for MFs 5–8 analyzes and the actual test data considering Case 1–4, respectively. Moreover, the testing performance values have been given in Table 14 for all cases presented in this study considering different numbers MF.

3.3. Comparison of performance of ANFIS with ANN

ANN was used to compare the performance of the ANFIS model for the prediction of the engine performance and emissions. The architecture of the ANN was shown in Fig. 18. ANN architecture used similar to

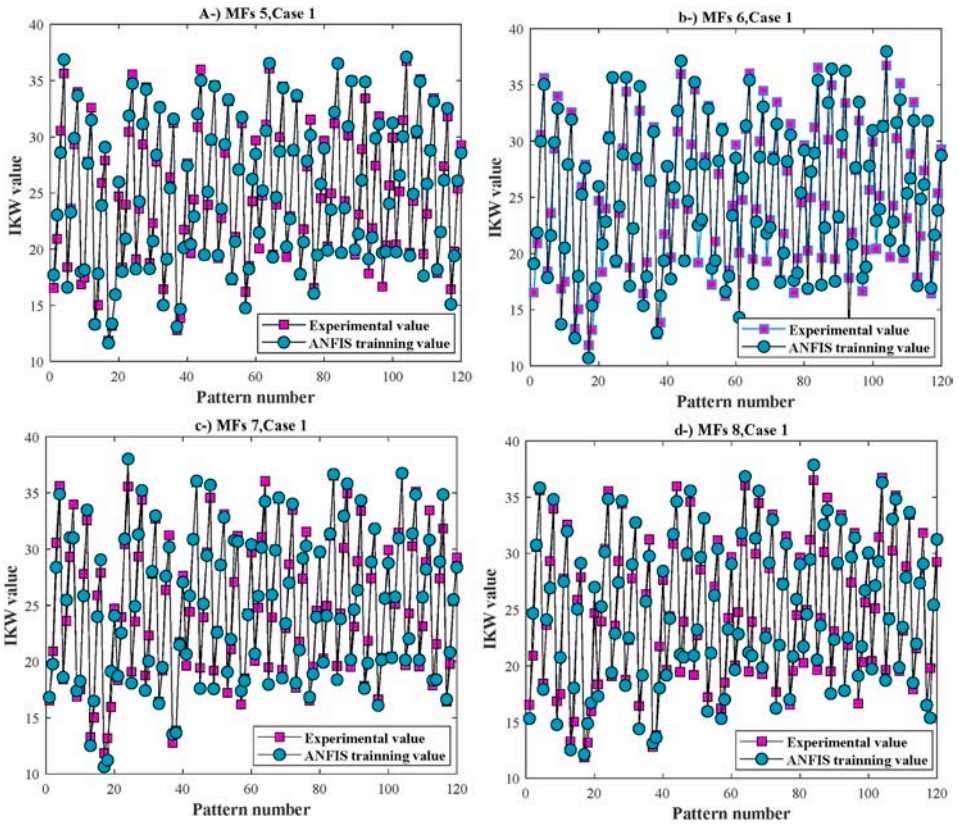

Fig. 10. The training performance of the ANFIS model used in this study considering four membership functions for Case 1 a-) MFs 5, b-) MFs 6, c-) MFs 7, MFs 8.

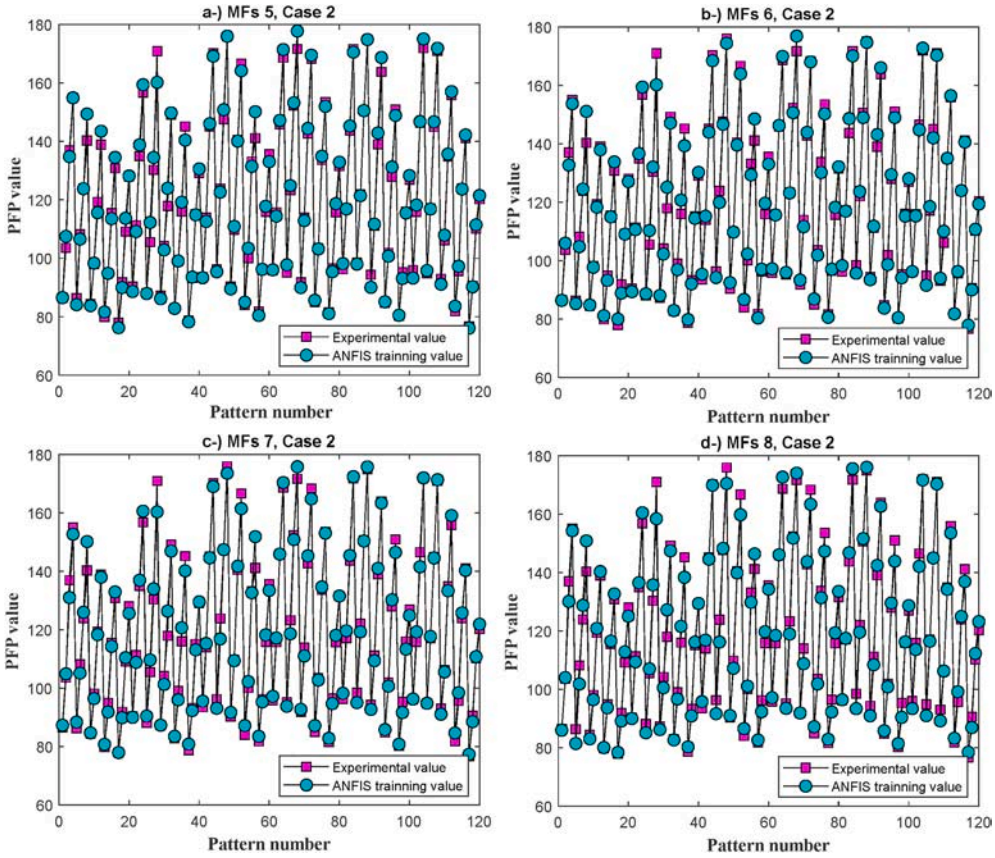

Fig. 11. The training performance of the ANFIS model used in this study considering four membership functions for Case 2 a-) MFs 5, b-) MFs 6, c-) MFs 7, MFs 8.

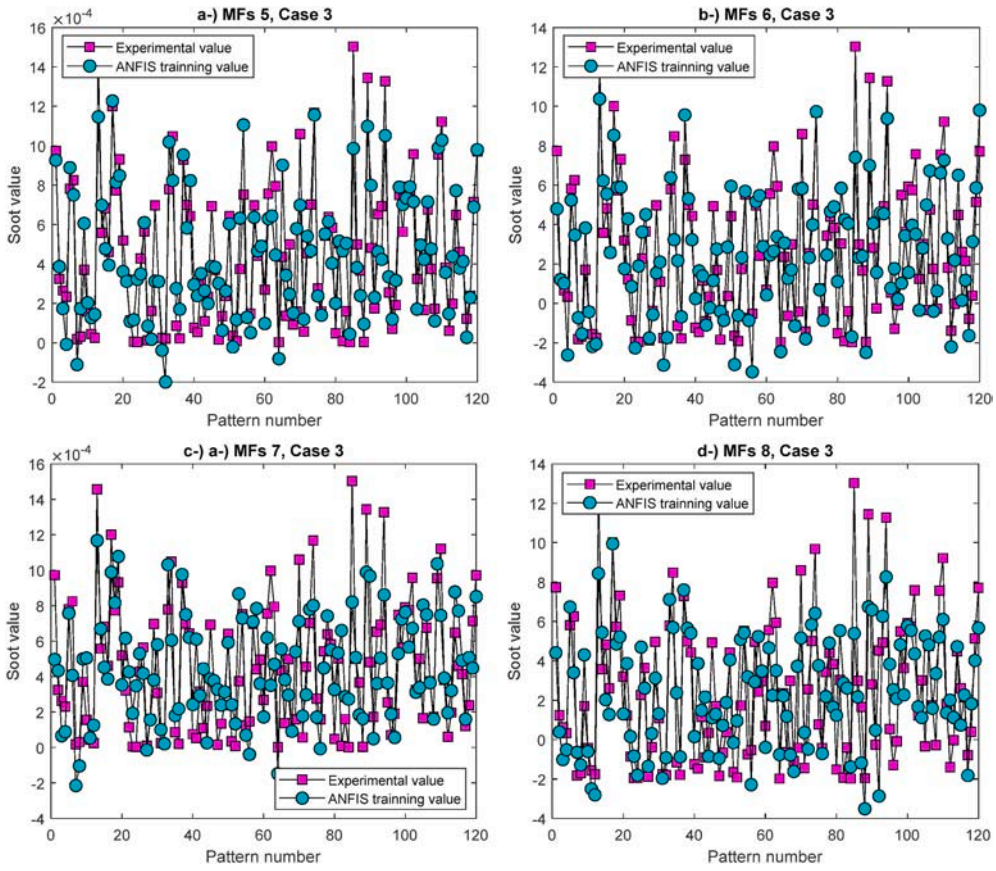

Fig. 12. The training performance of the ANFIS model used in this study considering four membership functions for Case 3 a-) MFs 5, b-) MFs 6, c-) MFs 7, MFs 8.

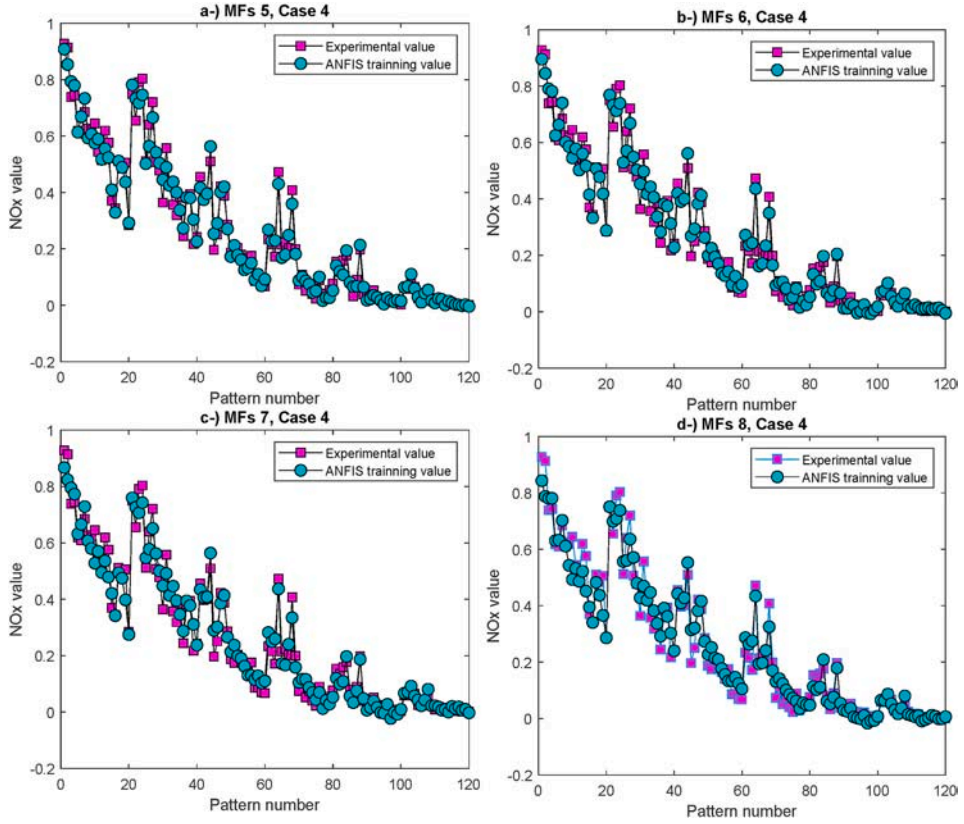

Fig. 13. The training performance of the ANFIS model used in this study considering four membership functions for Case 4 a-) MFs 5, b-) MFs 6, c-) MFs 7, MFs 8.

Table 10
The consequence parameters of the rules are defined end of the training process.

		Case 1					Case 2				
		p_i	q_i	r_i	w_i	s_i	p_i	q_i	r_i	w_i	s_i
300	MFs 5	0.059	0.456	0.342	−0.205	−0.757	−0.18	0.58	0.38	0.36	−0.46
	MFs 6	0.049	0.61	0.15	0.15	−0.27	−0.76	2.01	−0.57	0.27	0.38
	MFs 7	0.58	0.05	0.43	−0.74	−0.92	0.82	0.029	0.71	−0.22	0.12
	MFs 8	−0.888	−0.021	0.126	0.248	0.717	−0.82	0.478	0.20	1.06	−0.89
1200	MFs 5	–	–	–	–	–	–	–	–	–	–
	MFs 6	−0.0982	0.836	0.412	0.383	−0.92	0.53	−0.44	0.85	−0.25	−0.1005
	MFs 7	−0.792	0.826	0.125	0.548	−0.406	−0.871	0.865	0.67	1.05	0.19
	MFs 8	0.373	0.371	0.808	−0.44	−0.51	−0.39	2.12	0.29	1.70	−0.392
2000	MFs 5	–	–	–	–	–	–	–	–	–	–
	MFs 6	–	–	–	–	–	–	–	–	–	–
	MFs 7	−0.35	−0.59	0.45	0.55	−0.73	0.82	1.12	−0.023	0.75	0.209
	MFs 8	0.54	−0.36	−0.36	−0.72	0.079	−0.36	−0.60	−0.988	0.158	−0.411
4000	MFs 5	–	–	–	–	–	–	–	–	–	–
	MFs 6	–	–	–	–	–	–	–	–	–	–
	MFs 7	–	–	–	–	–	–	–	–	–	–
	MFs 8	0.3	−0.49	0.604	0.32	0.35	−0.0065	1.26	−0.097	0.578	−0.59

Table 11
The consequence parameters of the rules are defined end of the training process.

		Case 3					Case 4				
		p_i	q_i	r_i	w_i	s_i	p_i	q_i	r_i	w_i	s_i
300	MFs 5	−9.8e-5	−1.69e-5	9.42e-5	−2.1e-5	−2.5e-5	−0.0018	0.00074	−0.0034	0.00203	0.0027
	MFs 6	−4.4e-5	−5.14e-5	−1.8e-5	−3.6e-5	4.8e-5	−0.0034	0.00043	−0.00053	−0.0019	0.0024
	MFs 7	−5.4e-5	−7.1e-5	8.1e-6	8.6e-5	1e-05	−0.0018	0.0032	−0.0014	0.00129	0.0012
	MFs 8	5.26e-5	−1.5e-5	−4.3e-5	2.8e-5	−9.02e-5	−0.00156	0.0014	0.00314	−0.00117	0.0030
1200	MFs 5	–	–	–	–	–	–	–	–	–	–
	MFs 6	7.6e-5	1.7e-5	5.8e-6	−6.7e-5	−4.8e-5	0.0013	0.0029	0.0012	0.0010	0.0022
	MFs 7	−1.63e-5	1.8e-5	3.7e-5	−8.5e-5	8.8e-5	−0.00053	0.0036	0.0041	0.0043	0.0027
	MFs 8	−5.2e-6	1.2e-5	−2.7e-5	−3.9e-5	−5.5e-5	−0.00294	0.00072	−0.00035	−0.0029	−0.000705
2000	MFs 5	–	–	–	–	–	–	–	–	–	–
	MFs 6	–	–	–	–	–	–	–	–	–	–
	MFs 7	−3.2e-5	−2.2e-5	9.7e-5	−5.8e-5	5.4e-5	−0.0031	−0.00205	0.0012	0.0011	−0.000459
	MFs 8	3.3e-5	2.0e-5	−3.8e-5	4.4e-6	−6.5e-5	0.00109	0.0026	0.0011	−0.0012	0.00399
4000	MFs 5	–	–	–	–	–	–	–	–	–	–
	MFs 6	–	–	–	–	–	–	–	–	–	–
	MFs 7	–	–	–	–	–	–	–	–	–	–
	MFs 8	−6.9e-5	1.5e-5	−3.1e-5	9.1e-5	−5.6e-5	5.5e-6	−0.00018	0.0022	0.0041	0.0014

Table 12
The pattern in test sets used for the testing ANN.

	IP	TFM	EGR	SOI	IKW	PFP	SOOT	NO_X		IP	TFM	EGR	SOI	IKW	PFP	SOOT	NO_X
1	1.67	72.8	0	38	19.0	92.160	2.42e-4	6.3e-1	16	2.41	101.23	10	47	28.87	139.53	3.14e-04	3.34e-2
2	2.41	111.2	0	38	30.7	143.89	3.66e-4	7.0e-01	17	1.67	63.83	15	47	17.79	85.40	5.93e-04	3.31e-2
3	1.67	69.8	5	38	19.3	95.48	9.50e-4	4,2e-01	18	2,41	96.32	15	47	27,33	132,44	3.94e-04	2.37e-2
4	2.41	106.1	5	38	29.7	149.67	1.65e-5	4.1e-1	19	1.67	60.84	20	47	16.86	82.13	5.39e-04	1.23e-2
5	1.67	69.2	10	38	19.1	91.41	5.56e-4	3.4e-01	20	2.41	91.42	20	47	25.51	116.21	7.35e-04	1.22e-2
6	2.41	101.2	10	38	28.1	127.65	1.55e-5	4.5e-01	21	1.67	72.80	0	53	20.39	96.44	3.63e-04	5.28e-2
7	1.67	63.8	15	38	17.0	83.76	7.96e-4	2.6e-01	22	2.41	111.03	0	53	31.35	144.01	9.44e-06	2.01e-1
8	2.41	96.3	15	38	27.0	131.29	1.64e-4	1.8e-01	23	1.67	69.81	5	53	19.65	95.16	5.82e-05	2.20e-2
9	1.67	60.8	20	38	14.6	80.12	1.2e-3	2.2e-01	24	2.41	106.13	5	53	30.24	150.76	1.24e-04	6.54e-2
10	2.41	91.4	20	38	24.5	117.43	3.76e-4	1.2e-01	25	1.67	69.27	10	53	19.53	93.49	1.12e-03	2.74e-2
11	1.67	72.8	0	47	20.1	95.58	5.63e-4	1.7e-01	26	2.41	101.23	10	53	28.90	139.69	1.41e-04	2.77e-2
12	2.41	111.0	0	47	31.2	146.39	3.70e-6	2.1e-01	27	1.67	63.83	15	53	17.82	83.28	2.13e-04	6.67e-3
13	1.67	69.8	5	47	19.6	97.7	1.02e-3	7.3e-02	28	2.41	96.32	15	53	27.42	125.44	3.08e-04	1.27e-2
14	2.41	106.1	5	47	30.1	148.13	6.87e-4	7.3e-02	29	1.67	60.84	20	53	16.57	78.48	4.22e-04	4.92e-3
15	1.67	69.2	10	47	19.4	94.05	5.27e-4	9.5e-02	30	2.41	91.42	20	53	25.68	113.76	7.86e-04	3.68e-3

the ANFIS architecture in this study consists of three layers, an input layer, a hidden layer, and an output layer. There are four neurons in the input layer as IP, TFM, EGR, and SOI. In the hidden layer, four different neurons as 5, 6, 7, 8, were taken into consideration, comparison of ANFIS and ANN performance were analyzed. There was one neuron in the output layer to represent the output parameters for the four different cases (Table 6). This nervous was generated for the parameters of IKW, PFP, Soot, and NO_X. In order to activate the net input to the nervous in each layer, the sigmoid function was used. It was applied the generalized delta rule algorithm that includes forward and backward calculations from ANN calculation. The data were not processed in the input layer and the data were transferred to the hidden layer. The neurons in the hidden layer multiply the data transferred from the input layer with weights and calculate the net input. Then the data were calculated the output of the nervous using the activation function. This data is transmitted to the output laser and the same operations were repeated at the

Table 13
The testing set for the RCCI engine and comparison of results.

	Case 1 (%)				Case 2 (%)				Case 3 (%)				Case 4 (%)			
	MFs 5	MFs 6	MFs 7	MFs 8	MFs 5	MFs 6	MFs 7	MFs 8	MFs 5	MFs 6	MFs 7	MFs 8	MFs 5	MFs 6	MFs 7	MFs 8
1	0.97	8	5.1	2.3	1.3	0.44	0.9	1.3	98.2	98.1	160	129	4.4	5.2	4.1	3.5
2	12.4	3.8	5.2	7.6	0.4	3.1	1.9	3.1	16.4	361	494	337	12.8	11.1	9.8	11.9
3	8.4	3.4	3.2	0.1	0.6	2.2	1.4	1.6	64	141	9.6	36.8	17.6	18.1	18.7	16.5
4	4.9	3.4	7.2	5	0.11	0.15	1.03	0.82	49.7	61	9.5	87.8	4.3	2.9	3.9	2.1
5	0.01	4.3	8.9	5.8	3.7	3.9	3.5	7.1	89.1	61	60.6	55.1	13.1	5.9	0.31	4.4
6	4.92	7	3.5	9.2	4.3	6.4	7.8	9.2	16.1	54.5	1.3	4.6	1.5	4.2	6.7	7
7	4.9	5.2	2.3	4.1	3.4	6.4	5.4	4.7	1410	5.6	1152	273	32.6	30.4	28	26.4
8	0.35	6.7	6.4	1.6	2.2	3	3.1	5.04	709	3173	6450	7364	4.2	4.2	1.6	0.3
9	2	7.7	9.4	7.3	3.3	0.72	1.71	2.62	72.9	46.7	50.4	30.5	10.1	11.4	12	11
10	2.3	3.8	3.6	4.6	3.3	2.5	2	0.44	25.8	79.4	60.2	34.2	7.6	2.1	4.5	3.6
11	2.9	0.5	3.7	5.8	4	3.9	5.5	4.8	786	1116	1133	493	22.2	18.4	17.8	18.4
12	1.1	6.8	1	0.7	0.9	1.3	2.1	2.6	2485	175	99.3	2548	15.6	14.4	14.5	10.0
13	2.8	4.1	9.7	8.7	0.33	1.5	2.5	1.4	6	35.8	18.3	3.3	12.8	15.6	23.9	29.2
14	0.5	8.1	7.4	0.7	3.2	1.34	0.79	0.24	273	81	144	183	4.3	10.1	15.9	17.3
15	1.7	2	12.4	4	4.2	3.9	2.9	3.7	23.6	8.1	74.7	188	29.7	27.1	32.2	38
16	4.8	1.8	1.4	3.7	1.2	2.1	0.56	3.1	91	149	84	112	5.4	8.9	6.1	10.4
17	3.07	3	11.1	3.4	0.58	0.2	3.5	2	37.8	15.4	26.2	42.3	1.7	3.5	16.1	19.6
18	6.3	1.7	6.7	19.4	0.29	1	1.7	4.3	46.5	12.9	9.71	7.8	43.6	47.2	50	53.6
19	1.5	12.5	4.4	17.5	0.97	0.95	1.09	1.03	82	2.9	7.3	85	34.5	54.1	66	75.4
20	4.6	5.2	9.3	7.5	3.8	3.9	4.1	4.1	36.5	35.8	43.2	47.5	27.7	25.2	15.8	17
21	4.5	31.3	1.3	2.8	2.7	2.7	2.5	1.9	20.7	16.6	6.7	30	7	5.1	3.6	2.9
22	0.21	9.7	0.7	7.8	0.15	0.51	2.4	2.5	185	162	133	109	8.3	15	11.2	3.1
23	0.75	6.2	2.1	2	0.11	1.05	0.13	0.35	14500	20272	10302	14493	37.4	32	26.8	22.8
24	1.4	5.9	4.2	5.2	1.01	1.7	0.85	0.98	7090	3500	799	2861	28.2	31.4	31.9	35.1
25	1.06	17.5	7.1	7.2	0.97	1.14	3.22	3.7	11.2	22	28.1	38.9	57.2	33.9	28	47.6
26	0.73	9.1	6	8.5	1.58	1.8	2.42	1.86	31.2	20.4	69.3	40.3	20	3.1	15.6	17.2
27	2.3	1.9	4.9	6.4	3.1	2.1	2.4	3.2	71	28.7	69.3	87	80	77	81	85
28	1.2	3.8	0.5	0.8	1.2	1.5	1.6	1.8	453	24.6	141	779	103	97	80	71.3
29	5.41	0.49	1.1	5.4	4.2	0.49	1.02	2.4	71.9	77.5	55.4	50.3	19.5	8.2	9.07	2.2
30	6.9	3.1	4.7	3.9	2	1.1	0.02	1.6	12.1	20.6	5.05	3.5	1.1	14.8	13.2	61.6
31	5.39	2.9	9.6	0.4	4.1	3.9	3.6	3.6	37.2	38.9	79.5	22.6	22.2	0.93	29.1	94.5
32	3.48	0.16	4.5	1.4	4.3	2.5	0.52	0.09	5780	6238	3517	480	54	45	32	32
33	3.95	17.2	1.9	4.4	0.42	0.15	1.3	1.7	31.6	23.1	9.7	46.9	18.7	20.5	1.4	6.06
34	4.58	6.6	7	3	0.27	2.29	0.55	0.9	362	437	242	301	50.3	92.2	52.5	22.5
35	6.98	2.	3.2	5.3	1.7	1.8	0.64	0.98	19.9	8.4	34.7	56.3	49.5	45	93.2	17.8
36	5.23	0.57	3.5	1.1	1.3	0.5	0.75	2.22	58.1	3.9	76.5	3.61	81.1	36.2	19.9	30.2
37	8.8	6.9	4.8	10.7	0.82	1.7	0.29	0.39	16.9	43.4	64.5	20.2	57.9	170	329	187
38	0.61	8.2	4.1	14.2	2.14	0.67	3.2	4.9	17	30.1	6.2	4.6	68.3	111.	78.5	61.4
39	4.13	6.7	4.6	6	1.53	0.30	0.2	1.5	29.1	3.8	3.4	57.3	57	52.8	145	41.3
40	0.45	0.8	4.1	2.5	3.4	4.1	5.9	3.5	23.9	50.5	8.8	5.02	339	359	218	151
41	5.07	1.7	3	5.4	0.49	1	1.2	1.7	46.9	103	37	106	95	91.8	66.6	53.3
42	3.99	4.6	3.4	5.6	0.52	0.4	2.4	1.3	24.3	4.3	11.3	14.9	0.01	12.9	14.4	20.2
43	1.51	4	0.2	7	0.88	2.3	0.28	0.65	3576	3229	2596	4012	46.6	49.9	53.9	54.8
44	0.51	2	2.3	0.2	1.7	1.19	2.09	3.21	11949	8656	17169	7097	8.5	9.6	11.8	4.6
45	0.26	1.5	3.7	0.12	1.6	1.65	0.07	3.2	1071	1399	1312	1183	139	122	97.1	80.3
46	0.74	5.6	8.6	1	0.83	1.2	0.76	1.2	39.1	24.7	27.7	39.4	29.1	25.3	19.2	3.7
47	3.40	12.2	8	8.8	1.7	3.6	2.2	1.52	184	139	97.6	42.9	33.3	17.9	20.9	27.4
48	0.5	5.1	2.2	4.1	0.79	1.15	0.24	0.29	86.3	54.7	363	157	110	107	102	101
49	3.78	8.05	2.8	7.9	3.3	0.06	1.7	3.8	1.7	26.2	8.30	27.8	19.8	46.2	8.01	8.8
50	0.01	6.16	8.4	0.8	0.66	0.53	2.62	2.6	72.9	33.2	70.7	60.4	51.7	49.2	59.6	26.5
51	7.5	1.8	5.2	0.07	0.5	0.36	2.20	0.97	100	234	30.1	102	21.4	44.4	51.7	63.0
52	2.1	7.1	2.5	0.58	2	1.1	0.88	0.68	7.48	47.7	8.5	62.0	3.08	33.9	30.8	29.7
53	6.4	24.1	0.8	2.02	1.02	1.1	2.17	1.34	107	132	80.8	187	160	87.1	78.2	160
54	1.5	3.2	10.6	2.5	0.91	0.59	1.47	2	1615	1601	1525	1576	540.	10.	228	246
55	4.2	1.1	7.5	6.1	1.06	1.51	1.56	1.41	12.5	42.3	76.	47	44.1	51.3	46.6	119
56	1	5.2	5.2	3.6	3.1	3.24	1.19	0.29	39.2	11.6	3.81	36.2	17.8	50.0	99.2	2.86
57	10.5	4.3	0.19	8.9	0.27	1.25	0.88	1.78	59.7	68.9	83.2	36.5	243	5.1	127	198
58	1.9	0.09	5.6	6.6	0.35	0.24	2.07	3.54	60.3	8.6	41.9	61.7	520.	76.9	23.1	393.
59	3.1	2.7	2.8	0.79	0.7	0.4	1.9	0.39	3.27	34.2	21.9	28.5	233	94.9	38.2	231
60	2.83	1.5	2.9	3.3	0.41	0.74	1.74	0.69	85.4	36.1	79.6	70.8	3.34	41.4	11.7	62.7

output layer. The output of the nervous in the output layer is the output of the network. By comparing this output with the expected output, the error of the network is calculated. In order to reduce this error value, the backward calculation is performed using the generalized delta algorithm (Koç et al., 2016). The ANN architecture with five nervous in the hidden layer is shown in Fig. 18. Similarly, other ANN architectures were generated for performance comparison with ANFIS in this study (Table 15).

In Table 15, the comparison of the ANFIS performance with the ANN which architecture given in Fig. 18 has been explained according to MSE, R^2, and MEP parameters considering four different cases given in Table 5 and four different MFs used fuzzification of the input parameters. As shown in Table 15, when comparing the performance of the ANN and ANFIS, it is clearly shown that the training performance of the ANN is higher than ANFIS because the smallest MSE value is obtained as 1.23 in the ANFIS algorithm with MFs 5 situation, on the other hand, this value has been obtained as 0.32 in ANN algorithm with 4-8-1 architecture. Moreover, while the value of the parameter R^2 has been obtained as 0.998 in the training process with ANFIS MFs 5 situation, it was obtained as 0.999 with ANN 4-8-1 architecture. As can be seen, in Case

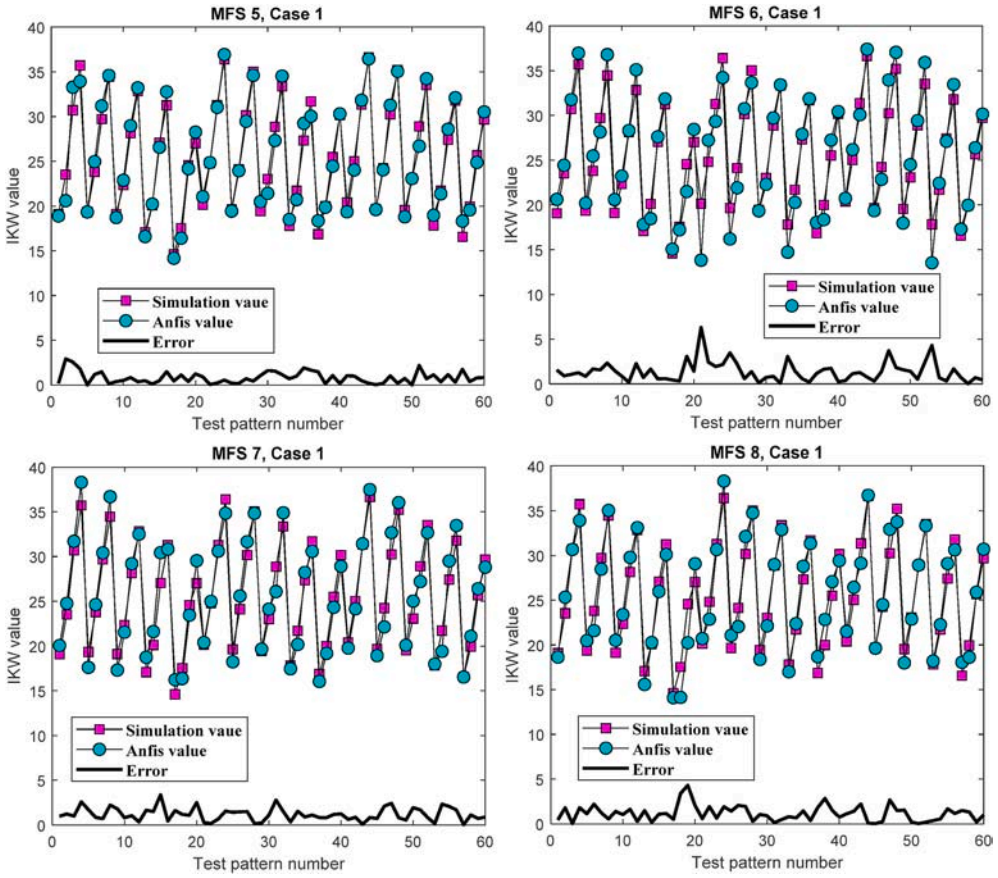

Fig. 14. The testing performance of the ANFIS model used in this study considering four membership functions for Case 1 a-) MFs 5, b-) MFs 6, c-) MFs 7, MFs 8.

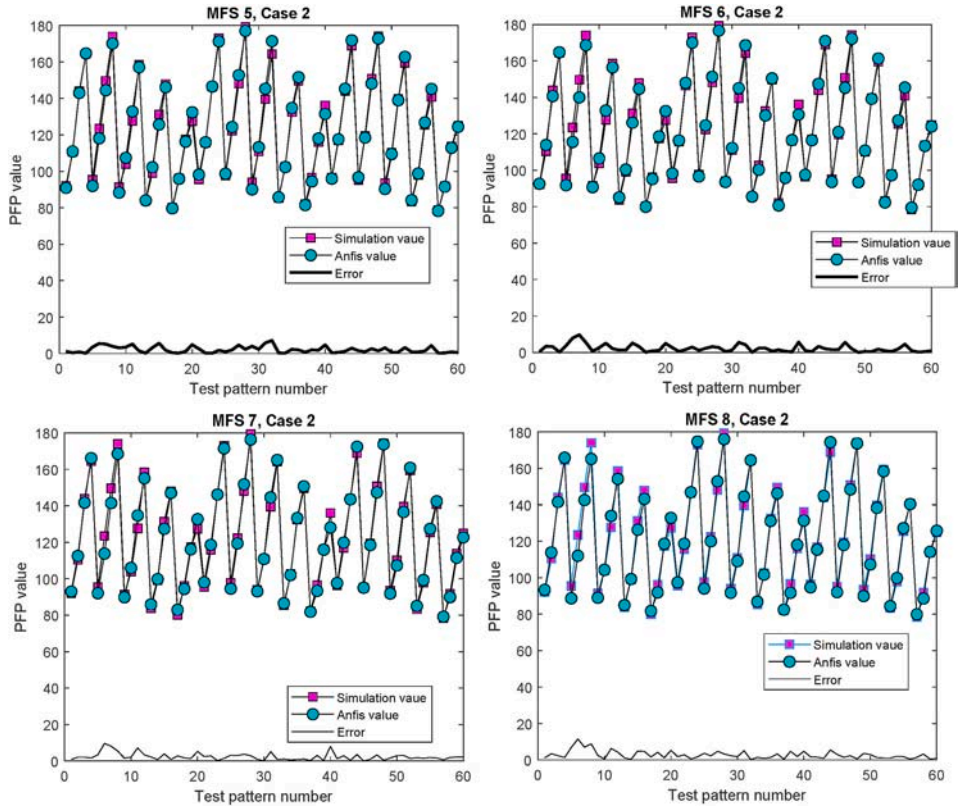

Fig. 15. The testing performance of the ANFIS model used in this study considering four membership functions for Case 2 a-) MFs 5, b-) MFs 6, c-) MFs 7, MFs 8.

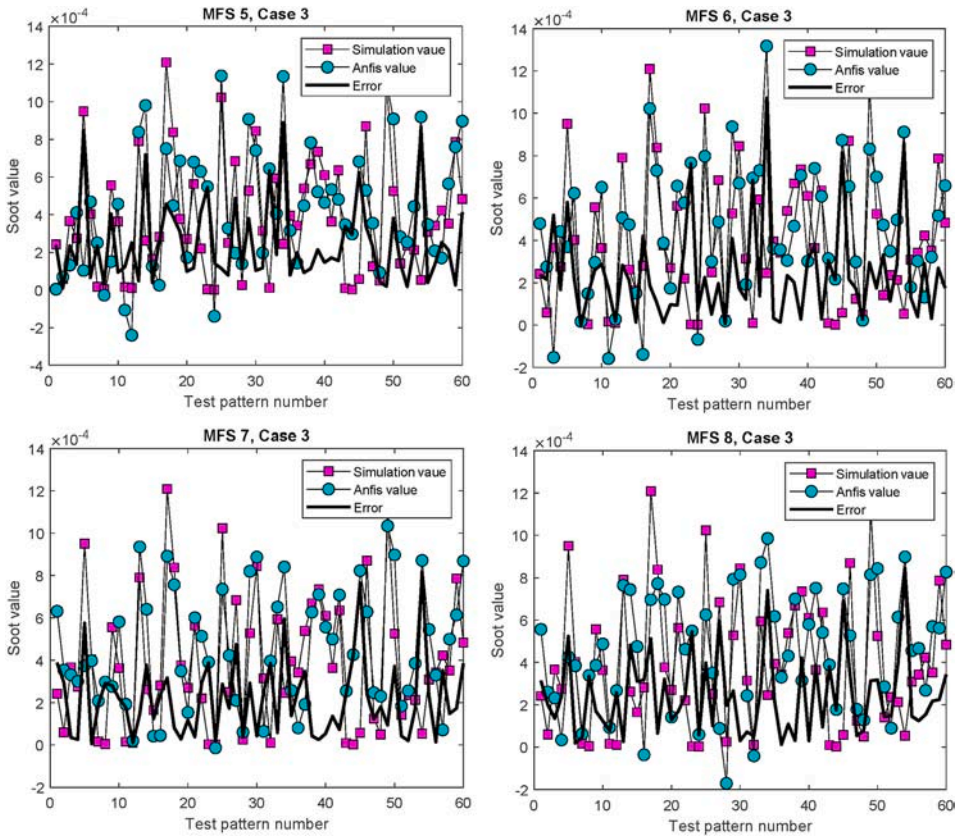

Fig. 16. The testing performance of the ANFIS model used in this study considering four membership functions for Case 3 a-) MFs 5, b-) MFs 6, c-) MFs 7, MFs 8.

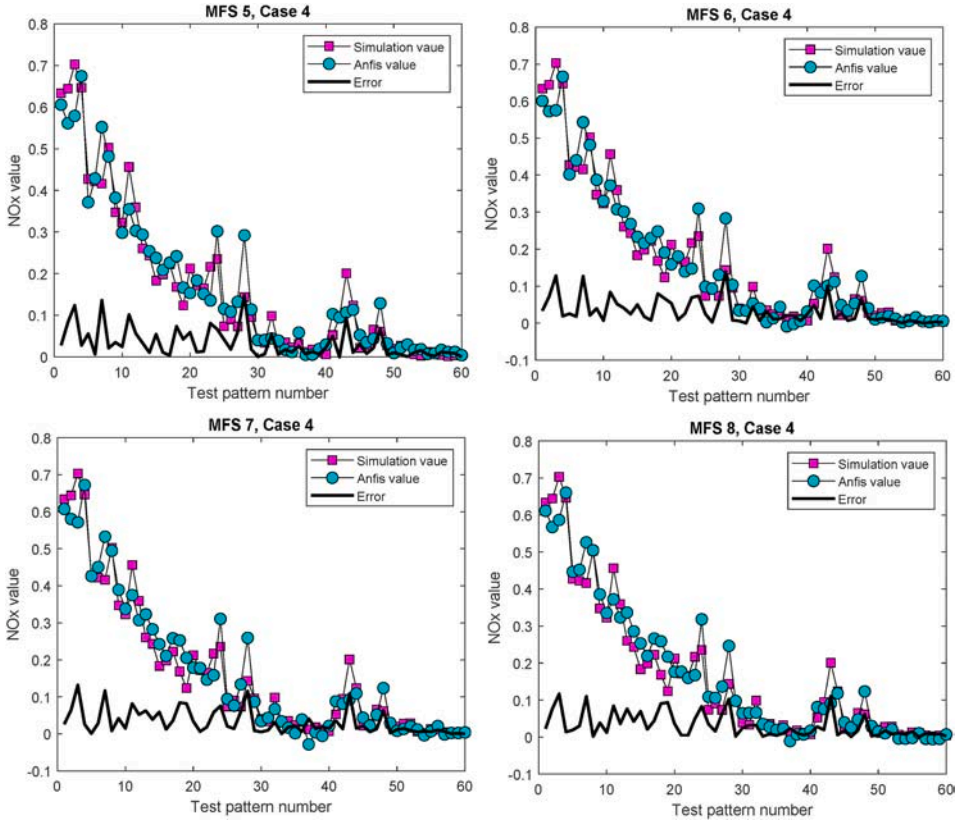

Fig. 17. The testing performance of the ANFIS model used in this study considering four membership functions for Case 4 a-) MFs 5, b-) MFs 6, c-) MFs 7, MFs 8.

Table 14
The testing performance of the ANFIS used in this study for the different cases.

	Case 1				Case 2			
	MFs 5	MFs 6	MFs 7	MFs 8	MFs 5	MFs 6	MFs 7	MFs 8
MSE	1.11	3.18	1.97	2.12	7.72	9.26	9.83	12.54
R^2	0.998	0.995	0.997	0.996	0.999	0.999	0.999	0.999
MEP	3.35	5.75	4.85	4.92	1.72	1.76	1.967	2.28
	Case 3				Case 4			
	MFs 5	MFs 6	MFs 7	MFs 8	MFs 5	MFs 6	MFs 7	MFs 8
MSE	1e-7	1e-7	8.0e-8	9.5e-8	0.0023	0.0021	0.0021	0.0021
R^2	0.55	0.55	0.67	0.6	0.9626	0.9654	0.9667	0.966
MEP	906	877	823	775	63.18	43.41	47.37	54.36

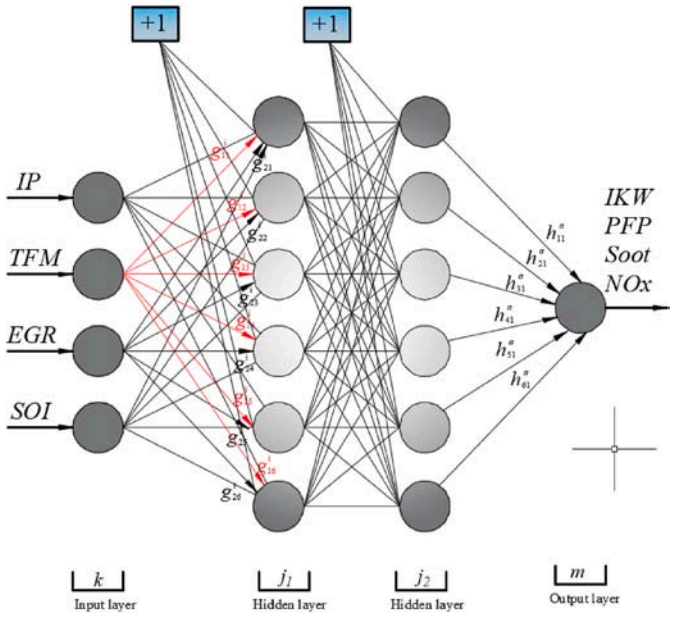

Fig. 18. ANN architecture used in this study.

1, the training performance of the ANN is more accurate than ANFIS. But the performance of an artificially intelligent algorithm must be evaluated according to testing performance, not training performance. When comparing testing performances of the ANN and ANFIS algorithms, it is clearly shown that the smallest MSE value is obtained as 1.11 in ANFIS with MFs 5 situation while this value is obtained as 1.62 in ANN 4-8-1 architecture. This result shows that testing performance ANFIS's performance is more accurate than ANN in terms of the test set given in Table 11. Otherwise, when comparing MEP values given in Table 15, a similar result was obtained as shown in Table 15.

Furthermore, when comparing the performance of the ANFIS and ANN algorithms for Case 2 given in Table 15, it is understood both the training and testing performance of the ANFIS model is more accurate according to ANN. While the smallest MSE value has been obtained as 6.901 in the ANFIS algorithm with MFs 6 situation in the training process, this value is obtained as 11.6 in ANN algorithm with 4-8-1 architecture. Moreover, the value of the parameter R^2 is very highly detected in both algorithms ($R^2 = 0.999$). when the comparing performances of the ANN and ANFIS algorithms for Case 2 given in Table 5, while the smallest MSE value has been achieved as 7.72 in ANFIS MFs 5, this value has been calculated as 53.27 in ANN with 4-5-1 architecture. Moreover, while the R^2 value has been calculated as 0.999 in the ANFIS algorithm, this is obtained as 0.996 in ANN. As shown in Table 15, the performance of the ANFIS and ANN algorithms is low in both the training and test process for Case 3 given in Table 5. The smallest MSE value has been calculated as 3.2e-8 and 8e-8 in the training and test process, respectively. This value is obtained as 4.9e-8 and 6e-8 for ANN in Case 3 considering training and test process, respectively. Apart from this, the biggest R^2 values have been obtained as 0.894 and 0.67 for the training and test performances of the ANFIS, respectively. On the other hand, these values have been obtained as 0.82 and 0.75 in the ANN algorithm, respectively. As shown in Table 15, in Case 4, according to a comparison of the performance of the ANFIS and ANN algorithms, in the training process, the smallest MSE values in ANFIS and ANN algorithms have been calculated as 0.001 for MFs 5 and 0.0022 for 4-8-1 architecture, respectively. Moreover, as shown in Table 15, the training performance of the ANFIS in Case 4 is higher than ANN as in Case 2. Moreover, when comparing R^2 parameters for the ANFIS and ANN algorithms, the biggest value has been calculated as 0.99 and 0.983 for the MFs 5 and 4-6-1 architecture, respectively. It is understood that the training performance of the ANFIS is better than ANN according to this comparison. When comparing the performances of the ANFIS and ANN for Case 4, the smallest MSE value has been obtained as 0.0021 and 0.0035, respectively. Furthermore, the biggest R^2 value is obtained as 0.9667 and 0.943 for the ANFIS and ANN, respectively. According to these values obtained from a comparison of the performance of the ANFIS and ANN, the prediction performance of the ANFIS is better than ANN.

4. Conclusions

The most important objective of an engine is to achieve maximum performance with minimum emission value due to increasingly tightening emission standards. The dual-fueled RCCI engine emits very low soot and NO_X emissions with high thermal efficiency. It is important to achieve low emissions in an RCCI engine under different loads and operating conditions. The main engine parameters that affect the exhaust emission are SOI, EGR, fuel mass, and intake pressure. Since the engine can be worked under different operating conditions, the emission value and engine parameters can also be different in varied conditions. In this study, the benefits of using ANFIS in terms of environmental pollution has been addressed as shown below:

- The prediction of emissions of an RCCI engine using ANFIS is a very important and useful technique for predetermining some critical parameters of the engine without lots of experimental effort. Thus, the sources can be used efficiently, and more economical results can be obtained.
- It is proven that using the artificially intelligent technique proposed in this study, it can be obtained critical parameters of the RCCI engine without any more experimental effort.

In order to define the relationship between input parameters to ANFIS and output parameters, the number of rules consisting of four different ANFIS cases was taken into consideration. Finally, by comparing the performance of the ANFIS model with ANN, the following results were obtained, respectively:

Table 15
Comparison of the ANFIS and ANN for the different cases.

		ANFS	ANFS	ANFS	ANFS	ANN	ANN	ANN	ANN
Case 1		MFs 5	MFs 6	MFs 7	MFs 8	4-5-1	4-6-1	4-7-1	4-8-1
MSE	Test	1.11	3.18	1.97	2.12	1.86	1.87	2.02	1.62
	Train	1.23	2.79	1.72	1.93	0.48	0.47	0.54	0.32
R^2	Test	0.998	0.995	0.997	0.996	0.997	0.997	0.997	0.997
	Train	0.998	0.995	0.997	0.997	0.999	0.999	0.999	0.999
MEP	Test	3.35	5.75	4.85	4.92	4.53	4.56	4.71	4.33
		ANFS	ANFS	ANFS	ANFS	ANN	ANN	ANN	ANN
Case 2		MFs 5	MFs 6	MFs 7	MFs 8	4-5-1	4-6-1	4-7-1	4-8-1
MSE	Test	7.72	9.26	9.83	12.54	53.27	62.4	66.05	56.1
	Train	6.93	6.901	8.62	12.21	17.38	17.94	13.2	11.6
R^2	Test	0.999	0.999	0.999	0.999	0.996	0.996	0.995	0.996
	Train	0.999	0.999	0.999	0.999	0.998	0.998	0.999	0.999
MEP	Test	1.72	1.76	1.967	2.28	3.85	3.9	3.72	3.7
		ANFS	ANFS	ANFS	ANFS	ANN	ANN	ANN	ANN
Case 3		MFs 5	MFs 6	MFs 7	MFs 8	4-5-1	4-6-1	4-7-1	4-8-1
MSE	Test	1e-7	1e-7	8.0e-8	9.5e-8	6.3e-8	6.17e-8	6e-8	6.56e-8
	Train	3.2e-8	4.85e-8	5.99e-8	5.92e-8	7.2e-8	7.1e-8	5.4e-8	4.9e-8
R^2	Test	0.55	0.55	0.67	0.6	0.74	0.72	0.75	0.73
	Train	0.894	0.838	0.7912	0.787	0.76	0.77	0.81	0.82
MEP	Test	906	877	823	775	270	376	260	368
		ANFS	ANFS	ANFS	ANFS	ANN	ANN	ANN	ANN
Case 4		MFs 5	MFs 6	MFs 7	MFs 8	4-5-1	4-6-1	4-7-1	4-8-1
MSE	Test	0.0023	0.0021	0.0021	0.0021	0.0036	0.0037	0.0035	0.0035
	Train	0.001	0.0014	0.0017	0.0023	0.0023	0.0023	0.0023	0.0022
R^2	Test	0.9626	0.9654	0.9667	0.966	0.942	0.94	0.943	0.943
	Train	0.990	0.988	0.985	0.981	0.982	0.983	0.982	0.982
MEP	Test	63.18	43.41	47.37	54.36	58.1	57.3	58.5	53.8

- In ANFIS and ANN algorithms, as the number of iterations increases, the MSE value gradually decreases while the R^2 value gradually increases. During the training, the minimum MSE and the maximum R^2 values in Case 1, 2, 3, 4 were obtained with MFs 5, MFs 6, MFs 5, MFs 5, respectively. According to this analysis, one can understand easily that optimum MFs number has been obtained variously for each simulation case given in Table 5.
- Considering the output of the ANFIS for the samples in the testing set, the minimum MSE and maximum R2 values for Case 1, 2, 3, 4 were also obtained in MFs 5, MFs 5, MFs 7, MFs 7.
- Lastly, the performance of the ANFIS model is compared with the ANN model. For Case 1, the training performance of ANN was higher than ANFIS. But considering the testing performance, the performance of ANFIS was higher than ANN. Similarly, In Cases 2 and 4, the testing and training performances of the ANFIS have been obtained as better than ANN according to Table 15.
- Only in Case 3, the testing performance of the ANN is better than ANFIS. But the training performance of the ANFIS is better than ANN as in Case 1, 2, and 4.

This study proves that an adaptive neuro-fuzzy based intelligent system is more effective than an artificial neural approach in terms of prediction of the emissions and performance parameters of the RCCI engine for the many simulation cases given the study because the ANFIS use both power of the fuzzification and learning capability together with the different number MF. Using experimental study and computational fluid dynamics approaches to obtain training and testing data, one can determine emission and performance characteristics of the RCCI engine without necessary costly and time-consuming laboratory studies. On the other hand, combined with the ANFIS, CFD, and experimental studies proposed in this study, the applications of RCCI engines will significantly reduce hazardous pollutants to achieve cleaner production and environmentally friendly on and off-road engines.

CRediT authorship contribution statement

Mehmet Akif Koç: Investigation, Conceptualization, Writing – original draft, Formal analysis, ANN and ANFIS analysis, Writing – review & editing. **Ramazan Şener:** Investigation, Conceptualization, Writing – original draft, Formal analysis, CFD analysis, Experimental validation, Writing – review & editing.

Declaration of competing interest

The authors declare that they have no known competing financial interests or personal relationships that could have appeared to influence the work reported in this paper.

Acknowledgments

The author (R. Şener) gratefully acknowledge Convergent Science Company for providing the academic version of the Converge CFD software.

Appendix A. Supplementary data

Supplementary data to this article can be found online at https://doi.org/10.1016/j.jclepro.2021.128642.

References

Ahmed, K., Ewees, A.A., El Aziz, M.A., Hassanien, A.E., Gaber, T., Tsai, P.-W., Pan, J.-S., 2017. A hybrid krill-ANFIS model for wind speed forecasting. In: Advances in Intelligent Systems and Computing, pp. 365–372. https://doi.org/10.1007/978-3-319-48308-5_35.

Al-qaness, M.A.A., Abd Elaziz, M., Ewees, A.A., Cui, X., 2019. A modified adaptive neuro-fuzzy inference system using multi-verse optimizer algorithm for oil consumption forecasting. Electronics 8, 1071. https://doi.org/10.3390/electronics8101071.

Alameer, Z., Elaziz, M.A., Ewees, A.A., Ye, H., Jianhua, Z., 2019. Forecasting copper prices using hybrid adaptive neuro-fuzzy inference system and genetic algorithms. Nat. Resour. Res. 28, 1385–1401. https://doi.org/10.1007/s11053-019-09473-w.

Altınkaya, H., Orak, İ.M., Esen, İ., 2014. Artificial neural network application for modeling the rail rolling process. Expert Syst. Appl. 41, 7135–7146. https://doi.org/10.1016/j.eswa.2014.06.014.
Amsden, A.A., 1997. KIVA-3V: A Block-Structured KIVA Program for Engines with Vertical or Canted Valves. LA Report.
Amsden, A.A., O'Rourke, P.J., Butler, T.D., 1989. KIVA-II: A Computer Program for Chemically Reactive Flows with Sprays. Los Alamos National Lab. https://doi.org/10.1007/BF01054829.
Atarod, P., Khlaife, E., Aghbashlo, M., Tabatabaei, M., Hoang, A.T., Mobli, H., Nadian, M. H., Hosseinzadeh-Bandbafha, H., Mohammadi, P., Roodbar Shojaei, T., Mahian, O., Gu, H., Peng, W., Lam, S.S., 2021. Soft computing-based modeling and emission control/reduction of a diesel engine fueled with carbon nanoparticle-dosed water/diesel emulsion fuel. J. Hazard Mater. 407, 124369. https://doi.org/10.1016/j.jhazmat.2020.124369.
Ağbulut, Ü., Ayyıldız, M., Sarıdemir, S., 2020. Prediction of performance, combustion and emission characteristics for a CI engine at varying injection pressures. Energy 197, 117257. https://doi.org/10.1016/j.energy.2020.117257.
Beale, J.C., Reitz, R.D., 1999. Modeling spray atomization with the Kelvin-Helmholtz/Rayleigh-Taylor hybrid model. Atomization Sprays. https://doi.org/10.1615/atomizspr.v9.i6.40.
Broatch, A., Olmeda, P., Margot, X., Escalona, J., 2019. New approach to study the heat transfer in internal combustion engines by 3D modelling. Int. J. Therm. Sci. 138, 405–415. https://doi.org/10.1016/j.ijthermalsci.2019.01.006.
Chen, Y., Zhu, Z., Chen, Y., Huang, H., Zhu, Z., Lv, D., Pan, M., Guo, X., 2020. Study of injection pressure couple with EGR on combustion performance and emissions of natural gas-diesel dual-fuel engine. Fuel 261, 116409. https://doi.org/10.1016/j.fuel.2019.116409.
Dharma, S., Hassan, M.H., Ong, H.C., Sebayang, A.H., Silitonga, A.S., Kusumo, F., Milano, J., 2017. Experimental study and prediction of the performance and exhaust emissions of mixed Jatropha curcas-Ceiba pentandra biodiesel blends in diesel engine using artificial neural networks. J. Clean. Prod. 164, 618–633. https://doi.org/10.1016/j.jclepro.2017.06.065.
Ebrahimi, M., Najafi, M., Jazayeri, S.A., 2018a. Artificial neural network to identify RCCI combustion mathematical model for a heavy-duty diesel engine fueled with natural gas and diesel oil. J. Braz. Soc. Mech. Sci. Eng. 40, 407. https://doi.org/10.1007/s40430-018-1328-9.
Ebrahimi, M., Najafi, M., Jazayeri, S.A., Mohammadzadeh, A.R., 2018b. A detail simulation of reactivity controlled compression ignition combustion strategy in a heavy-duty diesel engine run on natural gas/diesel fuel. Int. J. Engine Res. 19, 774–789. https://doi.org/10.1177/1468087417730486.
Ebrahimi, M., Najafi, M., Jazayeri, S.A., 2020. Multi-input–multi-output optimization of reactivity-controlled compression-ignition combustion in a heavy-duty diesel engine running on natural gas/diesel fuel. Int. J. Engine Res. 21, 470–483. https://doi.org/10.1177/1468087419832085.
Ewees, A.A., Aziz, M.A.E., Elhoseny, M., 2017. Social-spider optimization algorithm for improving ANFIS to predict biochar yield. In: 2017 8th International Conference on Computing, Communication and Networking Technologies (ICCCNT), pp. 1–6. https://doi.org/10.1109/ICCCNT.2017.8203950.
Gao, J., Tian, G., Ma, C., Xing, S., Huang, L., 2021. Numerical simulation on lean-burn characteristics of a naturally aspirated opposed rotary piston engine fuelled with hydrogen at wide open throttle conditions. J. Clean. Prod. 285, 124887. https://doi.org/10.1016/j.jclepro.2020.124887.
Gehmlich, R.K., Mueller, C.J., Ruth, D.J., Nilsen, C.W., Skeen, S.A., Manin, J., 2018. Using ducted fuel injection to attenuate or prevent soot formation in mixing-controlled combustion strategies for engine applications. Appl. Energy 226, 1169–1186. https://doi.org/10.1016/j.apenergy.2018.05.078.
Goztepe, K., 2013. Designing a battlefield fire support system using adaptive neuro-fuzzy inference system based model. Defence Sci. J. 63, 497–501. https://doi.org/10.14429/dsj.63.3716.
Han, Z., Reitz, R.D., 1995. Turbulence modeling of internal combustion engines using RNG k-ϵ models. Combust. Sci. Technol. 106, 267–295. https://doi.org/10.1080/00102209508907782.
Heywood, J., 1988. Internal Combustion Engine Fundamentals. McGraw Hill, New York.
Hosseini, M., Dalvand, A., 2014. Neural Network Approach for Estimation of Penetration Depth in Concrete Targets by Ogive-Nose. Steel Projectiles 492–506.
Huang, H., Lv, D., Zhu, J., Zhu, Z., Chen, Y., Pan, Y., Pan, M., 2019a. Development of a new reduced diesel/natural gas mechanism for dual-fuel engine combustion and emission prediction. Fuel 236, 30–42. https://doi.org/10.1016/j.fuel.2018.08.161.
Huang, H., Zhu, Z., Chen, Yingjie, Chen, Yajuan, Lv, D., Zhu, J., Ouyang, T., 2019b. Experimental and numerical study of multiple injection effects on combustion and emission characteristics of natural gas–diesel dual-fuel engine. Energy Convers. Manag. 183, 84–96. https://doi.org/10.1016/j.enconman.2018.12.110.
Jang, J.S.R., 1993. ANFIS: adaptive-network-based fuzzy inference system. IEEE Transact. Syst. Man Cybern. 23, 665–685. https://doi.org/10.1109/21.256541.
Kimura, S., Aoki, O., Kitahara, Y., Aiyoshizawa, E., 2001. Ultra-clean combustion technology combining a low-temperature and premixed combustion concept for meeting future emission standards. In: SAE Technical Papers. https://doi.org/10.4271/2001-01-0200.
Koide, R.M., Ferreira, A.P.C.S., Luersen, M.A., 2014. Laminated composites buckling analysis using lamination parameters, neural networks and support vector regression. Lat. Am. J. Solid. Struct. 12, 271–294.
Kokjohn, S.L., Hanson, R.M., Splitter, D.A., Reitz, R.D., 2011. Fuel reactivity controlled compression ignition (RCCI): a pathway to controlled high-efficiency clean combustion. Int. J. Engine Res. 12, 209–226. https://doi.org/10.1177/1468087411401548.
Koç, M.A., Esen, İ., Çay, Y., 2016. Tip deflection determination of a barrel for the effect of an accelerating projectile before firing using finite element and artificial neural network combined algorithm. Lat. Am. J. Solid. Struct. 13, 1968–1995. https://doi.org/10.1590/1679-78252718.
Kumar, S., Jain, S., Kumar, H., 2021. Application of adaptive neuro-fuzzy inference system and response surface methodology in biodiesel synthesis from jatropha–algae oil and its performance and emission analysis on diesel engine coupled with generator. Energy 226, 120428. https://doi.org/10.1016/j.energy.2021.120428.
Lagaros, N.D., Papadrakakis, M., 2012. Neural network based prediction schemes of the non-linear seismic response of 3D buildings. Adv. Eng. Software 44, 92–115. https://doi.org/10.1016/j.advengsoft.2011.05.033.
Liu, H., Yao, M., Zhang, B., Zheng, Z., 2008. Effects of inlet pressure and octane numbers on combustion and emissions of a homogeneous charge compression ignition (HCCI) engine. Energy Fuels. https://doi.org/10.1021/ef800197b.
Manuel, A., Gonzalez, D., Borman, G.L., Reitz, R.D., 1991. A study of diesel cold starting using both cycle analysis and multidimensional calculations. In: SAE Technical Papers. https://doi.org/10.4271/910180.
Mofijur, M., Hasan, M.M., Mahlia, T.M.I., Rahman, S.M.A., Silitonga, A.S., Ong, H.C., 2019. Performance and emission parameters of homogeneous charge compression ignition (HCCI) engine: a review. Energies 12, 3557. https://doi.org/10.3390/en12183557.
Mohan, B., Yang, W., Chou, S.K., 2013. Fuel injection strategies for performance improvement and emissions reduction in compression ignition engines - a review. Renew. Sustain. Energy Rev. https://doi.org/10.1016/j.rser.2013.08.051.
Najafi, G., Ghobadian, B., Moosavian, A., Yusaf, T., Mamat, R., Kettner, M., Azmi, W.H., 2016. SVM and ANFIS for prediction of performance and exhaust emissions of a SI engine with gasoline–ethanol blended fuels. Appl. Therm. Eng. 95, 186–203. https://doi.org/10.1016/j.applthermaleng.2015.11.009.
Najafi, B., Faizollahzadeh Ardabili, S., Mosavi, A., Shamshirband, S., Rabczuk, T., 2018. An intelligent artificial neural network-response surface methodology method for accessing the optimum biodiesel and diesel fuel blending conditions in a diesel engine from the viewpoint of exergy and energy analysis. Energies 11, 860. https://doi.org/10.3390/en11040860.
Nazemi, M., Shahbakhti, M., 2016. Modeling and analysis of fuel injection parameters for combustion and performance of an RCCI engine. Appl. Energy. https://doi.org/10.1016/j.apenergy.2015.11.093.
Nieman, D.E., Dempsey, A.B., Reitz, R.D., 2012. Heavy-duty RCCI operation using natural gas and diesel. SAE Int. J. Engines 5, 270–285. https://doi.org/10.4271/2012-01-0379.
Nordin, N., 1998. Numerical Simulations of Non-steady Spray Combustion Using a Detailed Chemistry Approach. Licentiate of Engineering thesis, Department of Thermo and Fluid Dynamics, Chalmers University of Technology, Goteborg, Sweden.
O'Rourke, P.J., 1989. Statistical properties and numerical implementation of a model for droplet dispersion in a turbulent gas. J. Comput. Phys. https://doi.org/10.1016/0021-9991(89)90123-X.
Pachiannan, T., Zhong, W., Rajkumar, S., He, Z., Leng, X., Wang, Q., 2019. A literature review of fuel effects on performance and emission characteristics of low-temperature combustion strategies. Appl. Energy 251, 113380. https://doi.org/10.1016/j.apenergy.2019.113380.
Perez-Ramirez, C.A., Amezquita-Sanchez, J.P., Adeli, H., Valtierra-Rodriguez, M., Camarena-Martinez, D., Romero-Troncoso, R.J., 2016. New methodology for modal parameters identification of smart civil structures using ambient vibrations and synchrosqueezed wavelet transform. Eng. Appl. Artif. Intell. 48, 1–12. https://doi.org/10.1016/j.engappai.2015.10.005.
Poorghasemi, K., Saray, R.K., Ansari, E., Irdmousa, B.K., Shahbakhti, M., Naber, J.D., 2017. Effect of diesel injection strategies on natural gas/diesel RCCI combustion characteristics in a light duty diesel engine. Appl. Energy. https://doi.org/10.1016/j.apenergy.2017.05.011.
Reitz, R.D., Ogawa, H., Payri, R., Fansler, T., Kokjohn, S., Moriyoshi, Y., Agarwal, A.K., Arcoumanis, D., Assanis, D., Bae, C., Boulouchos, K., Canakci, M., Curran, S., Denbratt, I., Gavaises, M., Guenthner, M., Hasse, C., Huang, Z., Ishiyama, T., Johansson, B., Johnson, T.V., Kalghatgi, G., Koike, M., Kong, S.C., Leipertz, A., Miles, P., Novella, R., Onorati, A., Richter, M., Shuai, S., Siebers, D., Su, W., Trujillo, M., Uchida, N., Vaglieco, B.M., Wagner, R.M., Zhao, H., 2020. IJER editorial: the future of the internal combustion engine. Int. J. Engine Res. https://doi.org/10.1177/1468087419877990.
Richards, K.J., Senecal, P.K., Pomraning, E., 2019. CONVERGE 2.4 Manual.
Rogers, S.K., Colombi, J.M., Martin, C.E., Gainey, J.C., Fielding, K.H., Burns, T.J., Ruck, D.W., Kabrisky, M., Oxley, M., 1995. Neural networks for automatic target recognition. Neural Network. 8, 1153–1184. https://doi.org/10.1016/0893-6080(95)00050-X.
Sada, S.O., Ikpeseni, S.C., 2021. Evaluation of ANN and ANFIS modeling ability in the prediction of AISI 1050 steel machining performance. Heliyon 7, e06136. https://doi.org/10.1016/j.heliyon.2021.e06136.
Salahi, M.M., Gharehghani, A., 2019. Control of combustion phasing and operating range extension of natural gas PCCI engines using ozone species. Energy Convers. Manag. 199, 112000. https://doi.org/10.1016/j.enconman.2019.112000.
Saravanakumar, L., Prakash, R., 2020. Validation of performance and emissions of a CI engine fueled with calophyllum inophyllum methyl esters using soft computing technique. Fuel 266, 117070. https://doi.org/10.1016/j.fuel.2020.117070.
Schmidt, D.P., Rutland, C.J., 2000. A new droplet collision algorithm. J. Comput. Phys. https://doi.org/10.1006/jcph.2000.6568.
Senecal, P.K., Pomraning, E., Richards, K.J., Briggs, T.E., Choi, C.Y., McDavid, R.M., Patterson, M.A., 2003. Multi-dimensional modeling of direct-injection diesel spray liquid length and flame lift-off length using cfd and parallel detailed chemistry. In: SAE Technical Papers. https://doi.org/10.4271/2003-01-1043.

Şener, R., Gül, M.Z., 2021. Optimization of the combustion chamber geometry and injection parameters on a light-duty diesel engine for emission minimization using multi-objective genetic algorithm. Fuel 304, 121379. https://doi.org/10.1016/j.fuel.2021.121379.

Sener, R., Yangaz, M.U., Gul, M.Z., 2020. Effects of injection strategy and combustion chamber modification on a single-cylinder diesel engine. Fuel 266, 117122. https://doi.org/10.1016/j.fuel.2020.117122.

Shu, J., Fu, J., Liu, J., Ma, Y., Wang, S., Deng, B., Zeng, D., 2019. Effects of injector spray angle on combustion and emissions characteristics of a natural gas (NG)-diesel dual fuel engine based on CFD coupled with reduced chemical kinetic model. Appl. Energy 233 (234), 182–195. https://doi.org/10.1016/j.apenergy.2018.10.040.

Singh, N.K., Singh, Y., Sharma, A., Abd Rahim, E., 2020a. Prediction of performance and emission parameters of Kusum biodiesel based diesel engine using neuro-fuzzy techniques combined with genetic algorithm. Fuel 280, 118629. https://doi.org/10.1016/j.fuel.2020.118629.

Singh, N.K., Singh, Y., Sharma, A., Kumar, S., 2020b. Diesel engine performance and emission analysis running on jojoba biodiesel using intelligent hybrid prediction techniques. Fuel 279, 118571. https://doi.org/10.1016/j.fuel.2020.118571.

Splitter, D., Wissink, M., Kokjohn, S., Reitz, R.D., 2012. Effect of compression ratio and piston geometry on RCCI load limits and efficiency. In: SAE Technical Papers. SAE International. https://doi.org/10.4271/2012-01-0383.

Taghavifar, Hadi, Taghavifar, Hamid, Mardani, A., Mohebbi, A., Khalilarya, S., Jafarmadar, S., 2016. Appraisal of artificial neural networks to the emission analysis and prediction of CO2, soot, and NOx of n-heptane fueled engine. J. Clean. Prod. 112, 1729–1739. https://doi.org/10.1016/j.jclepro.2015.03.035.

Taqizadeh, A., Jahanian, O., Kani, S.I.P., 2020. Effects of equivalence and fuel ratios on combustion characteristics of an RCCI engine fueled with methane/n-heptane blend. J. Therm. Anal. Calorim. 139, 2541–2551. https://doi.org/10.1007/s10973-019-08669-9.

Walker, N.R., Wissink, M.L., DelVescovo, D.A., Reitz, R.D., 2015. Natural gas for high load dual-fuel reactivity controlled compression ignition in heavy-duty engines. J. Energy Resour. Technol. Transact. ASME 137, 1–7. https://doi.org/10.1115/1.4030110.

Yadav, A.K., Gaur, P., 2016. Neuro-Fuzzy-based improved IMC for speed control of nonlinear heavy duty vehicles. Defence Sci. J. 66, 665. https://doi.org/10.14429/dsj.66.9489.

Yue, Z., Reitz, R.D., 2019. Application of an equilibrium-phase spray model to multicomponent gasoline direct injection. Energy Fuels 33, 3565–3575. https://doi.org/10.1021/acs.energyfuels.8b04435.